Curvature in Biological Systems: Its Quantification, Emergence, and Implications across the Scales

Barbara Schamberger, Ricardo Ziege, Karine Anselme, Martine Ben Amar, Michał Bykowski, André P. G. Castro, Amaia Cipitria, Rhoslyn A. Coles, Rumiana Dimova, Michaela Eder, Sebastian Ehrig, Luis M. Escudero, Myfanwy E. Evans, Paulo R. Fernandes, Peter Fratzl, Liesbet Geris, Notburga Gierlinger, Edouard Hannezo, Aleš Iglič, Jacob J. K. Kirkensgaard, Philip Kollmannsberger, Łucja Kowalewska, Nicholas A. Kurniawan, Ioannis Papantoniou, Laurent Pieuchot, Tiago H. V. Pires, Lars D. Renner, Andrew O. Sageman-Furnas, Gerd E. Schröder-Turk, Anupam Sengupta, Vikas R. Sharma, Antonio Tagua, Caterina Tomba, Xavier Trepat, Sarah L. Waters, Edwina F. Yeo, Andreas Roschger,* Cécile M. Bidan,* and John W. C. Dunlop*

Surface curvature both emerges from, and influences the behavior of, living objects at length scales ranging from cell membranes to single cells to tissues and organs. The relevance of surface curvature in biology is supported by numerous experimental and theoretical investigations in recent years. In this review, first, a brief introduction to the key ideas of surface curvature in the context of biological systems is given and the challenges that arise when measuring surface curvature are discussed. Giving an overview of the emergence of curvature in biological systems, its significance at different length scales becomes apparent. On the other hand, summarizing current findings also shows that both single cells and entire cell sheets, tissues or organisms respond to curvature by modulating their shape and their migration behavior. Finally, the interplay between the distribution of morphogens or micro-organisms and the emergence of curvature across length scales is addressed with examples demonstrating these key mechanistic principles of morphogenesis. Overall, this review highlights that curved interfaces are not merely a passive by-product of the chemical, biological, and mechanical processes but that curvature acts also as a signal that co-determines these processes.

1. Introduction

Biological materials develop into a variety of complex shapes, which can respond and adapt their form as they interact with their physical environment. Remodeling in bone, the formation of reaction wood in trees, and humidity-dependent shape changes in seed-capsules being just some examples. Recent technical advances allow detailed studies of cells, microorganisms, and the tissues they form, as well as their interaction with complex in vivo or in vitro environments. These studies showed that living systems have developed a wide range of mechanisms that enable them not only to sense and react to their physical environment, but also to modify and control their immediate surroundings.[1] This field of mechanobiology[2] has started to raise new questions about the role of geometry and in particular, the role of local curvature in biological

B. Schamberger, V. R. Sharma, A. Roschger, J. W. C. Dunlop
Department of the Chemistry and Physics of Materials
Paris-Lodron University of Salzburg
5020 Salzburg, Austria
E-mail: andreas.roschger@plus.ac.at; john.dunlop@sbg.ac.at

The ORCID identification number(s) for the author(s) of this article can be found under https://doi.org/10.1002/adma.202206110.

R. Ziege, A. Cipitria, M. Eder, P. Fratzl, C. M. Bidan
Department of Biomaterials
Max Planck Institute of Colloids and Interfaces
14476 Potsdam, Germany
E-mail: cecile.bidan@mpikg.mpg.de

K. Anselme, L. Pieuchot
IS2M (CNRS - UMR 7361)
Université de Haute-Alsace
F-68100 Mulhouse, France

K. Anselme, L. Pieuchot
Université de Strasbourg
F-67081 Strasbourg, France

M. Ben Amar
Department of Physics
Laboratoire de Physique de l'Ecole Normale Supérieure
24 rue Lhomond, 75005 Paris, France

M. Bykowski, Ł. Kowalewska
Department of Plant Anatomy and Cytology
Faculty of Biology
University of Warsaw
02-096 Warsaw, Poland

A. P. G. Castro, P. R. Fernandes, T. H. V. Pires
IDMEC
Instituto Superior Técnico
Universidade de Lisboa
1049-001 Lisboa, Portugal

A. P. G. Castro
ESTS
Instituto Politécnico de Setúbal
2914-761 Setúbal, Portugal

A. Cipitria
Group of Bioengineering in Regeneration and Cancer
Biodonostia Health Research Institute
20014 San Sebastian, Spain

A. Cipitria
IKERBASQUE
Basque Foundation for Science
48009 Bilbao, Spain

R. A. Coles
Cluster of Excellence, Matters of Activity
Humboldt-Universität zu Berlin
10178 Berlin, Germany

R. Dimova
Department of Theory and Bio-Systems
Max Planck Institute of Colloids and Interfaces
14476 Potsdam, Germany

S. Ehrig
Max Delbrück Center for Molecular Medicine
13125 Berlin, Germany

S. Ehrig
Berlin Institute for Medical Systems Biology
10115 Berlin, Germany

L. M. Escudero, A. Tagua
Instituto de Biomedicina de Sevilla (IBiS)
Hospital Universitario Virgen del Rocío/CSIC/Universidad de Sevilla and
Departamento de Biología Celular
Universidad de Sevilla
41013 Seville, Spain

L. M. Escudero, A. Tagua
Biomedical Network Research Centre on Neurodegenerative Diseases (CIBERNED)
28031 Madrid, Spain

M. E. Evans
Institute for Mathematics
University of Potsdam
14476 Potsdam, Germany

L. Geris
Biomechanics Research Unit
GIGA In Silico Medicine
University of Liège
4000 Liège, Belgium

N. Gierlinger
Institute of Biophysics
Department of Nanobiotechnology
University of Natural Resources and Life Sciences Vienna (Boku)
1190 Vienna, Austria

E. Hannezo
Institute of Science and Technology Austria
3400 Klosterneuburg, Austria

A. Iglič
Laboratory of Physics
Faculty of Electrical engineering
University of Ljubljana
Tržaška 25, SI-1000 Ljubljana, Slovenia

J. J. K. Kirkensgaard
Condensed Matter Physics
Niels Bohr Institute
University of Copenhagen
Universitetsparken 5, 2100 København Ø, Denmark

J. J. K. Kirkensgaard
Ingredients and Dairy Technology
Department of Food Science
University of Copenhagen
Rolighedsvej 26, 1958 Frederiksberg, Denmark

P. Kollmannsberger
Center for Computational and Theoretical Biology
University of Würzburg
97074 Würzburg, Germany

N. A. Kurniawan
Department of Biomedical Engineering and Institute for Complex Molecular Systems
Eindhoven University of Technology
5600 MB Eindhoven, The Netherlands

I. Papantoniou
Prometheus Division of Skeletal Tissue Engineering
KU Leuven
O&N1, Herestraat 49, PB 813, 3000 Leuven, Belgium

I. Papantoniou
Skeletal Biology and Engineering Research Center
Department of Development and Regeneration
KU Leuven
O&N1, Herestraat 49, PB 813, 3000 Leuven, Belgium

I. Papantoniou
Institute of Chemical Engineering Sciences
Foundation for Research and Technology (FORTH)
Stadiou Str., 26504 Patras, Greece

L. D. Renner
Leibniz Institute of Polymer Research and the Max Bergmann Center of Biomaterials
01069 Dresden, Germany

A. O. Sageman-Furnas
Department of Mathematics
North Carolina State University
Raleigh, NC 27695, USA

G. E. Schröder-Turk
School of Physics
Chemistry and Mathematics
Murdoch University
90 South St, Murdoch, WA 6150, Australia

G. E. Schröder-Turk
Department of Materials Physics
Research School of Physics
The Australian National University
Canberra, ACT 2600, Australia

A. Sengupta
Physics of Living Matter
Department of Physics and Materials Science
University of Luxembourg
L-1511 Luxembourg City, Grand Duchy of Luxembourg

C. Tomba
Univ Lyon
CNRS
INSA Lyon
Ecole Centrale de Lyon
Université Claude Bernard Lyon 1
CPE Lyon, INL, UMR5270, 69622 Villeurbanne, France

2206110 (2 of 23)

**ADVANCED
SCIENCE NEWS**

www.advancedsciencenews.com

**ADVANCED
MATERIALS**

www.advmat.de

systems. Although many ideas can be traced back to authors such as D'Arcy Thompson,[3] important technical developments in microfabrication, imaging, and computation have brought them to the forefront. The implications of curvature on biology span multiple length scales. Recent work has shown that single cells located on curved surfaces can sense and respond to local curvature.[4] At larger length scales, processes controlling the formation of living tissues, such as extracellular matrix (ECM) secretion or cellular proliferation, strongly depend on geometrical aspects.[5] Among the many reviews about interactions between curvature and biology, more specific ones cover: the role of membrane curvature in cell biology,[6] into how cells, cell sheets, or tissues sense and react to curvature,[7] and how nature harnesses wrinkling and buckling as mechanisms to create complex and functional shapes.[8] Although some mechanisms of curvature emergence are specific to a certain length scale, other mechanisms have commonalities that are scale-independent, operating in a wide range of systems spanning from the sub-cellular to the organ scale. The present review aims to highlight how these fundamental mechanisms act on membranes, animal and plant cells, microorganisms, and during organ development. A broad selection of examples will highlight how different biological systems trigger and react to curvature changes. The challenges of measuring and prescribing curvature are multi-fold. Mathematical and computational tools are needed to describe curvature of surfaces in 3D from the discrete and noisy data coming from experiments.[9] Surface manufacturing techniques need to be improved or even developed to create well-defined 3D geometries and patterns that can be used in experiments. And finally, profound biological and biophysical knowledge is required to design and interpret experiments, which allow observing the emergence and the effect of curvature in in vitro conditions. Clearly, these challenges demand a highly interdisciplinary approach that requires mathematicians, computer scientists, physicists, engineers, and biologists to combine forces and work together on addressing these questions. Therefore, biologists exchange with mathematicians to develop image quantification software, biophysicists design experimental setups with material scientists, and physicists develop 3D live imaging methods compatible with the requirements specifications of biologists.[10] To enable such close collaborations and knowledge transfer across fields, it appears crucial to establish a common background with the basics from the different disciplines, and to agree on a common language. The first objective of this review is thus to provide the readers with the minimum knowledge required from mathematics, mechanics, biology, and imaging (**Table 1**, Sections 2 and 3) to understand the emergence and the implications of

curvature in biology (Sections 4–6). The ideas and concepts presented in this paper result from discussions held in a series of workshops by the name "CurvoBio" held in Salzburg and online in 2019, 2020 and 2021.

2. Describing the Curvature of a 2D Surface

Compared to experiments on planar surfaces, the study of biological processes on curved surfaces introduces significant complexity that is not only related to the experiment itself but also to the choice of techniques and algorithms used to measure and extract curvature information from 3D samples. In the following subsections, we discuss how these choices can be made. The appropriate formulation of curvature depends on the type of biological problem. For example, the total curvature of a finite surface patch is most useful to describe the growth of a leaf, while principal curvatures and asymptotic directions, which are defined locally at a point on the surface, are needed to describe the motion of cells confined to a curved substrate. We will describe here a simple way of considering the total curvature of a surface, using the so-called Steiner Offset, as well as the local curvature at a point on the surface through the more well-known principal curvature directions.

2.1. Total Curvature of a Surface Patch

A natural notion of total curvature relates to how the area of a surface grows or shrinks as one moves to a surface parallel to the original surface: a surface parallel to a flat plane will have the same area, whereas a surface parallel to a curved surface will have significantly more area. Consider first a 1D curve in a 2D plane. When a segment of a 1D curve f with positive total curvature H_{2D} in a 2D plane is offset from its original position by a (small) distance t along the local normal to the curve N (see **Figure 1**, left), the length of the arc increases from L_0 to L, according to the linear equation $L = L_0 + H_{2D}t$. This means that a line segment with greater curvature will have a parallel offset that grows more quickly in length compared to a segment with less curvature.

The same is true for a 2D surface, however the growth of the offset surface now has both a linear term and a quadratic term, which leads to a more nuanced notion of total curvature, including both total mean and total Gaussian curvatures. Generalizing this to a 2D surface patch in 3D space (Figure 1, right), the surface area of the parallel surface (A) can be written as $A = A_0 + 2Ht + Kt^2$, where A_0 is the surface area of the original surface patch. The linear term H is the total (or integral) mean curvature and the quadratic term, K is the total (or integral) Gaussian curvature of the surface patch. This concept of describing curvature through length or area change is known as the Steiner Offset.

The Steiner Offset formulation of total curvature of a surface patch helps explain how membrane shape is determined by the geometry of the constituent molecules.[6b,14] If we consider a lipid bilayer having a mid-surface, then the headgroups of the lipids lie on parallel surfaces to that surface, offset by a value of t and $-t$, where t is the approximate height of the lipid

X. Trepat
ICREA at the Institute for Bioengineering of Catalonia
The Barcelona Institute for Science and Technology
08028 Barcelona, Spain

X. Trepat
Centro de Investigación Biomédica en Red en Bioingeniería
Biomateriales y Nanomedicina (CIBER-BBN)
08028 Barcelona, Spain

S. L. Waters, E. F. Yeo
Mathematical Institute
University of Oxford
OX2 6GG, Oxford, UK

Table 1. Glossary: Some important concepts to understand the role of curvature in biology.

Term	Description	Illustration
Mathematics		
Principal curvatures	$\kappa_1 = \frac{1}{R_1}$, $\kappa_2 = \frac{1}{R_2}$ are the minimal and maximal curvatures at a point on a surface	
Local Gaussian curvature	$\kappa_K = \kappa_1 \kappa_2$	
Local mean curvature	$\kappa_H = \frac{(\kappa_1 + \kappa_2)}{2}$	
Steiner's formulation	Surface area of a parallel surface (A), which depends on the total mean (H) and total Gaussian (K) curvature $A = A_0 + 2Ht + Kt^2$	
Mechanics		
Stress	Force per unit of area $\sigma = \frac{F}{A}$	
Strain	Deformation relative to the initial length $\varepsilon = \frac{\Delta l}{l_0}$	
Young's Modulus	Slope of the reversible or elastic region of a stress–strain curve $E = \frac{\Delta \sigma}{\Delta \varepsilon}$	
Poisson's ratio	Negative ratio of lateral strain to the strain along the loading direction $\nu_{xy} = -\frac{\varepsilon_x}{\varepsilon_y}$	
Biology		
Mechanosensing	Translation of mechanical force to facilitate a biochemical response. For example, focal adhesions (FAs, transmembrane protein complexes) transmit mechanical signals from the surrounding to the intracellular space. FAs bind to actin, which is together with myosin, a contractile element of the cytoskeleton. Actin can bind to linker of nucleoskeleton and cytoskeleton (LINC), a complex of transmembrane proteins located at the nuclear membrane. The LINC is connected to the nuclear lamina, which in turn can influence transcription factors.[1] Another possible mechanism is the activation of mechanosensitive ion channels by forces.[11]	DNA / Actomyosin network / Focal Adhesions / Nuclear Lamina / LINC / Mechanosensitive ion channels
Curvotaxis	Cellular migration guided by surface curvature[4b]	
Extracellular matrix (ECM)	A network surrounding the cells including components like collagen or fibronectin[12]	

molecule. Steiner's formulation of curvature dictates that the local area change of the surfaces through the tail groups and the head groups of the molecules implies a particular Gaussian curvature of the membrane. The emergent Gaussian curvature properties of the membrane can be well described using this formulation (see Section 4.2). **Figure 2** shows a few examples
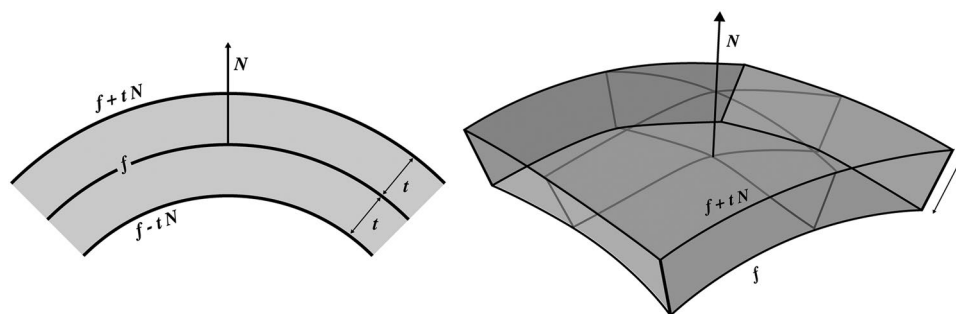

Figure 1. Illustration of the Steiner Offset for a line segment (left) and a surface patch (right). Adapted with permission.[13] Copyright 2019, The Author.
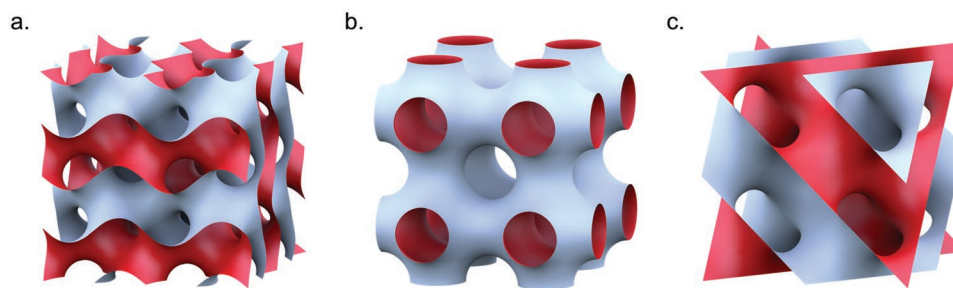
Figure 2. Examples of three triply periodic minimal surfaces. a) Gyroid, b) primitive cubic surface, and c) diamond cubic surface. Adapted with permission.[16] Copyright 2014, Walter de Gruyter Berlin/Boston.

of surfaces having zero mean curvature at all points on the surface due to a local minimization of the surface area, which have been identified in biological membranes: the gyroid, primitive, and diamond cubic surfaces (from left to right in Figure 2).[6b,15] As these structures can be generated by translating a cubic unit cell in the three spatial directions, they are also called triply periodic minimal surfaces.

The sign of Gaussian curvature gives information about the shape: a sphere-like surface patch will have positive Gaussian curvature, a flat or cylindrical surface patch will have zero Gaussian curvature, and a negative Gaussian curvature indicates a hyperbolic surface (saddle-like) patch (**Figure 3**a). According to the Gauss–Bonnet theorem, the total Gaussian curvature of a closed surface in 3D space is a topological invariant of the surface. In essence, the topology is characterized by the number of "holes" in the closed surface (examples from 0 to 3 are given in Figure 3b).[17]

Another important consequence of Gaussian curvature can be seen in the parallel transport theorem (**Figure 4**): surfaces of nonzero total Gaussian curvature cannot be covered by a set of lines that are everywhere parallel. This effect has immediate consequences for any process that involves the movement or alignment of objects on a curved surface. It means, e.g., that ECM materials or even polarized cells cannot be perfectly aligned everywhere on nonzero total Gaussian curvature surfaces. Local alignment however remains possible, meaning that defects such as disclinations and grain boundaries may appear to separate regions of local alignment. The physics of the generation of such defects is very rich, see, e.g., ref. [18] and there is evidence that topological defects may indeed influence individual cell and tissue behavior (e.g., ref. [19], see also Section 6).

2.2. Curvature at a Point on a Surface

While the notion of total mean and Gaussian curvature over a surface patch is convenient in the description of emergent curvature in biological systems, such as membrane curvature, it is also useful to describe curvature at a point on the surface (or an infinitesimally small patch). In 2D, the curvature of the curve at point P can be understood by constructing an osculating circle, with the same tangent vector as the curve at P. The curvature is then the inverse of the radius (r) of this circle, $\kappa(P) = \frac{1}{r}$. The sign of κ depends on the side of the curve on which the osculating circle resides (**Figure 5**a). The generalization to surfaces in 3D is shown in Figure 5b. Curvature can be defined for the

a. total Gaussian curvature of surfaces

$K > 0$ $K = 0$ $K < 0$
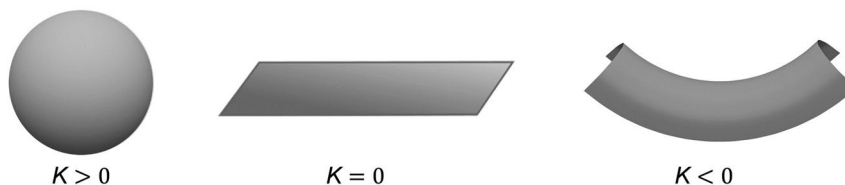
b. total Gaussian curvature of closed surfaces

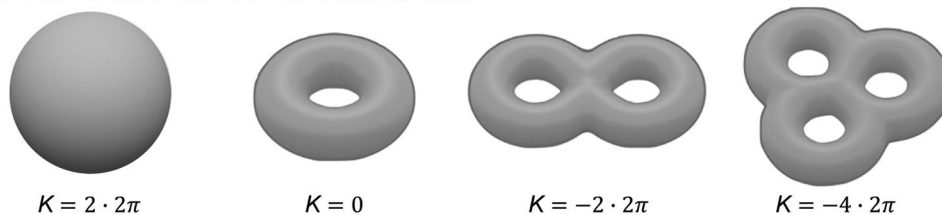$K = 2 \cdot 2\pi$ $K = 0$ $K = -2 \cdot 2\pi$ $K = -4 \cdot 2\pi$

Figure 3. a) Examples of surfaces with positive (left), zero and negative (right) total Gaussian curvatures. b) Illustrations of closed surfaces and their respective total Gaussian curvature.
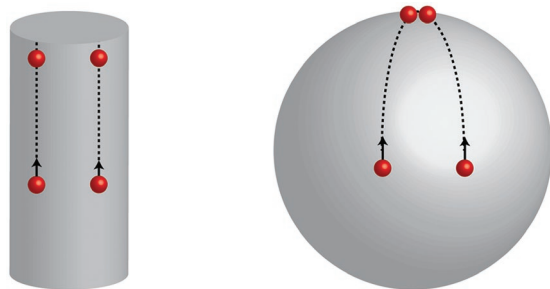
**ADVANCED
SCIENCE NEWS**
www.advancedsciencenews.com

**ADVANCED
MATERIALS**
www.advmat.de

Figure 4. A cylinder and a sphere have, respectively, zero and nonzero positive Gaussian curvatures. Two particles moving parallel to each other on a cylinder (zero Gaussian curvature surface) will never collide. However, particles moving parallel to each other on a nonzero Gaussian surface (e.g., sphere) will converge (or diverge for negative Gaussian curvature surfaces).

curve in any cutting plane that contains the normal vector $\vec{n}$ to the surface at P (Figure 5a,b). The maximum and the minimum values of this curvature are known as the principal curvatures, κ_1 and κ_2 (Figure 5b-iii,iv). The pointwise mean curvature κ_H at a point P is given by the average of the two principal curvatures,

$$\kappa_H = \frac{(\kappa_1 + \kappa_2)}{2},$$ and the pointwise Gaussian curvature is the product of the two principal curvatures, $\kappa_K = \kappa_1 \kappa_2$. Summing the pointwise mean and Gaussian curvatures in a small area patch recovers the total mean curvature (H) and the total Gaussian curvature (K) appearing in the Steiner Offset formula for surfaces given in the previous section. Functions given as combinations of the principal curvatures may also describe the influence of curvature more readily than the mean or Gaussian curvatures. For example, for a membrane containing anisotropic inclusions, the curvature is usually described by a curvature deviator $\kappa_D = (\kappa_1 - \kappa_2)/2 = (\kappa_H^2 - \kappa_K)^{1/2}$.[20]

3. Measuring and Quantifying Curvature

Using curvature measurements to describe the shape of biological samples or objects is not trivial due to the discrete nature of the measurement data and the feature sizes that might appear on different length scales. A broad range of methods based on different physical principles is available to obtain 3D describing an object's shape (**Figure 6**a). For example, Figure 6b shows microcomputed tomography scans from a raspberry represented as discrete voxels where the voxel brightness allows to differentiate foreground (material) from background. When introducing curvature measurements as done above (see Section 2), we assume that the curves or surfaces are "smooth," meaning that they do not have kinks or corners (as it is the case for a voxel-based dataset). Hence, only an approximation of the raspberry surface via smooth surface patches allows consistent notions of curvature to be derived using changes in lengths, areas, and normal or tangential directions, which are readily computed by repeated differentiation.

There is no single or best way to define curvatures for discrete representations of objects. Instead, one harnesses a toolbox of definitions and constructions depending on research perspectives, questions, and goals. Consider the simplest example of a 1D curve in a 2D plane. For a smooth curve, we used two different approaches to discuss the curvature, one compares the length of parallel offset curves, giving the total curvature as the change of length for a fixed normal distance, the other measures pointwise by comparing the curvature with that of the osculating circles. In the smooth case, these approaches lead to a consistent definition of curvature. For a polygonal curve, however, each of these approaches leads to its own definition of curvature.[21] Hence, for the raspberry in our example this means that curvature measurements on smooth and discrete representation of the surface will lead to different results even though the same object is described.
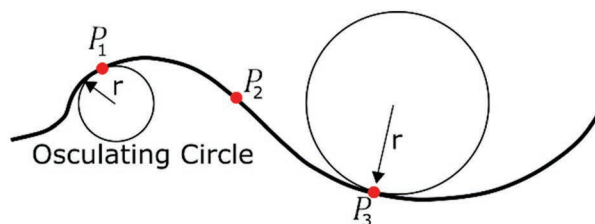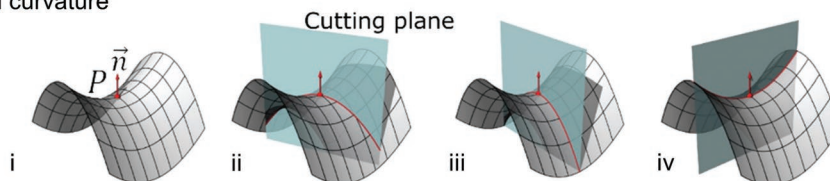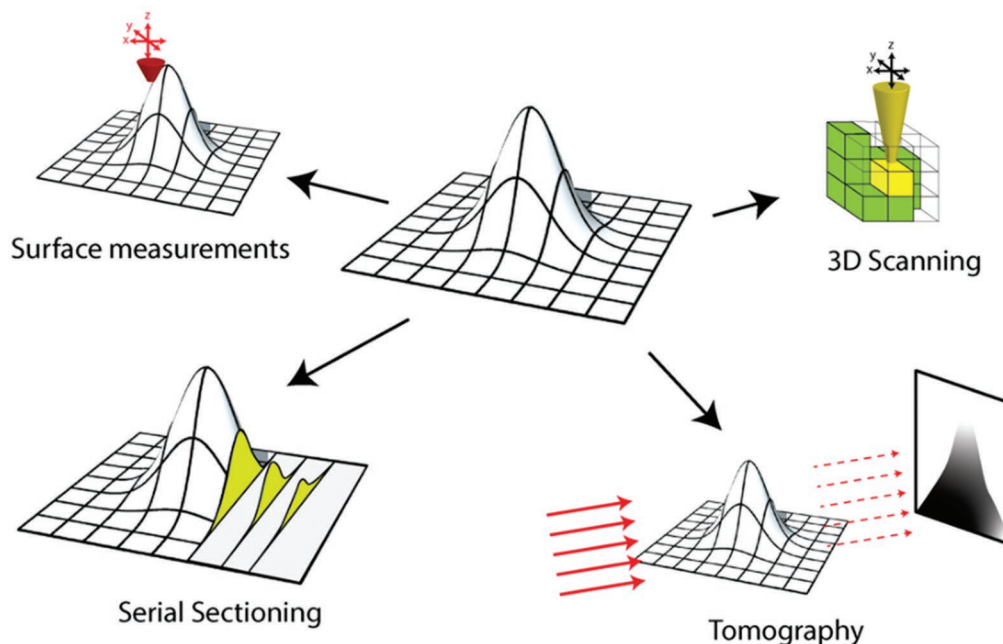

Figure 5. a) The curvature of a 2D curve is given by the inverse of the radius of a best approximating circle (osculating circle) that has the same tangent vector as the curve at a given point. Moving along the curve from the point P_1 to P_2, the curvature decreases to zero and then the osculating circle changes sides giving a negative curvature at the point P_3. b) i) For a surface embedded in 3D, the normal curvature at a point P can be measured by measuring the curvature of ii) the curve (in red) defined by the intersection of a cutting plane (light blue) containing the normal vector $\vec{n}$ with the surface. The curve and therefore its normal curvature depend on the angle of rotation around the normal vector. For any point on a surface (with the exception of points where the curvature is the same in all directions), there are two extremal values of normal curvature, the principal curvatures: iii) maximal κ_1 and iv) minimal κ_2.

2206110 (6 of 23)

**ADVANCED
SCIENCE NEWS**

www.advancedsciencenews.com

**ADVANCED
MATERIALS**

www.advmat.de

a. experimental techniques to measure surface curvature

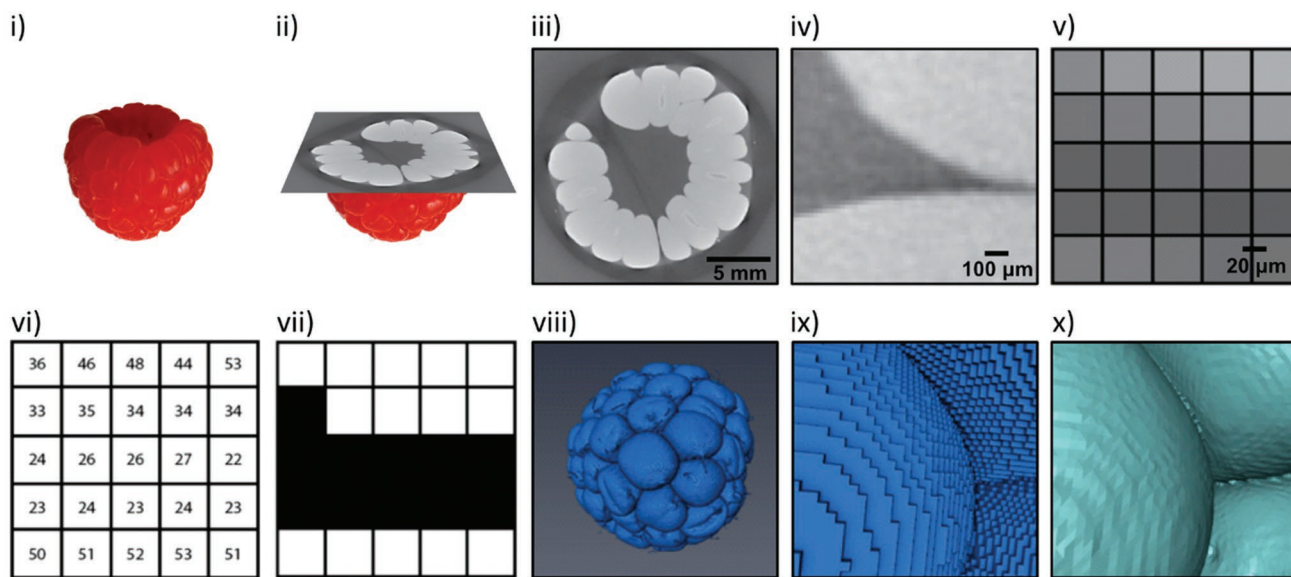## b. steps from experimental data towards surface mesh

Figure 6. a) Experimental techniques to measure 3D geometry. (Clockwise from top left) Applied methods range from approaches that measure directly the coordinates of a surface, such as atomic force microscopy (AFM), to full 3D scanning methods such as confocal microscopy, to methods that rely on multiple images of projections (tomography), to serial sectioning such as focused ion beam scanning electron microscopy (FIB SEM). b) Main steps to derive a mash representing an object's surface illustrated via i) the example of a raspberry, going from discrete images coming from computed tomography data ii–v) to a surface mesh and eventually surface curvature. vi) Typically, an image consists of a discrete pixel or voxel-based grid where each pixel/voxel is assigned to the intensity of a given signal. This image can be vii) converted by thresholding and binarization to vii, ix) a voxel-based data set, x) which can be fitted with a triangulated surface mesh.

Broadly speaking, discrete data can be interpreted: i) as a "discretization" of a smooth shape, where definitions of curvature are seen as approximate at each finite resolution when measured against a smooth limit shape, or ii) as an exact

determination of a polygonal shape, where definitions of curvature preserve some structure at all finite resolutions but it may be difficult to measure against a smooth limit shape. The former includes analytic and computational methods from the study of partial differential equations,[22] while the latter encompasses the emergent field of discrete differential geometry and its applications in computer graphics.[23] Current research in pure and applied mathematics draws on the strength of both interpretations and also seeks robust methods to address the added challenge of noisy real-world data.[24]

3D datasets from biological samples (from the sub-cellular to organ level) can originate from a wide range of techniques, e.g., fluorescence microscopy (confocal, light sheet), macro- and microcomputed tomography, magnetic resonance imaging, and much more (Figure 6a). These methods vary in their applicability, whether they are destructive or not and whether they are fast enough and noninvasive so they can be used to image living systems.[25] Surface-based methods, such as the extremely sensitive atomic force microscopy or scanning near-field microscopy are limited to nonoverhanging surfaces. Full 3D scanning methods such as laser-scanning confocal microscopy or light-sheet microscopy give the intensity of a signal (e.g., fluorescence) in a 3D volume. Tomographic methods measure the angle-dependent attenuation of a signal passing through the entire sample. Projections are then reconstructed into the entire 3D volume.[26] Finally, the destructive method of serial sectioning and imaging, exemplified by focused ion beam scanning electron microscope, allows high-resolution reconstruction of 3D data. Although the resolution and the type of obtained information depend on the underlying physics of the employed method, all methods, except for the surface-based approaches, have in common that the output data are represented by a discrete voxel-based 3D matrix (equivalent to a stack of 2D pixelated images). Each element of this array corresponds to the value of the local physical measurement of, e.g., material density, dye concentration, mineral content, etc. Data quality is influenced by the presence of measurement artefacts, contrast, image noise, and resolution of the method. Once such a data set is obtained, the 3D array needs to be processed to extract quantitative parameters about the geometry of the objects measured.

There are several ways to obtain information on the shape and local curvature from experimental 3D datasets. The most common approach involves: image filtering to reduce noise and measure artifacts (Figure 6b-iii,iv), thresholding and binarization, i.e., separation into foreground and background based on the location of iso-intensity-surfaces or edges (Figure 6b-v–vii), and conversion of the voxel-based data (Figure 6b-viii,ix) into a surface mesh (Figure 6b-x). Finally, a local evaluation of the surface mesh properties/orientations can be performed to obtain curvature information. The final step requires algorithms that can give a measure of curvature on the mesh itself. One such method uses information about the normal vectors of each face on a triangular mesh to estimate an operator (the so-called Weingarten operator), which in turn directly allows the determination of principal curvatures.[27] Local curvature estimates on a triangulated mesh are especially important for 3D renderings of smooth surfaces. This often implies either the conversion of a mesh into a tangent vector field, which allows adding

texture onto curved surfaces,[28] or using principles of mesh area minimization to model smooth constant mean curvature shapes.[29] As experimental data are usually noisy, smoothing techniques (e.g., kd-tree median filtering or diffusion kernels) can be used as described in ref. [30].

An alternative to using surface meshes is to directly calculate geometric information from voxel-based datasets. Such approaches avoid thresholding and segmentation steps and apply convolutions directly to the intensity images, thus avoiding potential errors and artifacts. Local brightness gradients in the 3D images can be used to determine surfaces and corresponding normal vectors,[31] and from these estimates of curvature can be obtained. This approach however requires data smoothing (e.g., 3D Deriche filters[32]) to reduce noise and to ensure differentiability of the data at every point.

Image data can also be used to parametrize a mathematical approximation of the object in which the curvature can be analytically determined. In 2D, splines have been used to determine tissue curvature of epithelial cell layers, but this is more challenging in 3D.[33] Spherical harmonics have been used to approximate drosophila embryo shape from light-sheet data.[34]

These examples illustrate the diversity of approaches and the inherent difficulty in measuring curvature of biological systems. Many algorithms are available as open-source tools and are reviewed and compared in terms of efficiency and accuracy in refs. [9b,35]. In general, gradient-based algorithms are faster but sometimes less accurate than mesh-based approaches. The quality of the results strongly depends on the specific algorithm but also on the complexity of the evaluated structure and the starting format (voxel or mesh). It must not be forgotten that real measurement data always contain noise, partial volume effects, and other artifacts, which can only be partially removed by filtering. As these contributions potentially alter curvature evaluation, the final precision of the curvature estimate depends on the resolution of the selected method, statistical robustness (leveraging multiple replicates), the quality of the obtained data, and the applied evaluation algorithm.

4. Curvature Emergence in Biology

Curvature in biological systems typically emerges from an adaptation to physical boundary conditions and is omnipresent at all length scales. Depending on the feature size and the spatial resolution of the experimental method, the description of the local curvature of natural objects can be challenging, but investigating how a living system generates shape is even more complex. This is especially the case when considering the feedback between the biological system itself with the physical boundaries of the environment. Hence, to obtain a comprehensive picture of cell behavior and ECM organization, the mechanical forces causing shape changes as well as biological aspects of how the system reacts to those need to be considered. Indeed, mechanical factors such as the presence of tensile/compressive stresses from an external boundary, the elastic modulus of the surrounding environment, or adhesive stress, are more and more recognized for their crucial role in tissue shaping and function, as in the brain,[47] where even neuronal communication would be driven by mechanical forces.[48]

2206110 (8 of 23)

The shape of a surface is of course coupled to its physical behavior, with mechanical loading due to pressure or tension changing the surface geometry. One example illustrating the link between curvature and physics is the Laplace–Young equation, $\Delta p = 2\gamma \kappa_H$, which relates the pressure difference, Δp, over an interface with mean curvature, κ_H, to its surface tension, γ.[49] This implies that at equilibrium, a fluid at constant pressure will be bound by a surface with constant mean curvature. Despite its simplicity, this equation can give rise to considerable complexity in equilibrium surfaces as is known from our everyday observations of soap bubbles.[50] In general, changes in mean and Gaussian curvature can be linked to changes in the mechanical energy via the so-called Helfrich Hamiltonian

$$E = \oint \left(k_b \left(\frac{1}{2}\kappa_H^2 - \kappa_0 \kappa_H \right) + k_s \kappa_G \right) dA \qquad (1)$$

where k_b is the bending modulus, k_s is the stretching modulus, and κ_0 is the spontaneous curvature.[51] The spontaneous curvature can be thought of as the curvature a patch of a thin membrane or sheet takes if it is under no external constraint. Any change relative to this state will lead to an energy increase. This concept, e.g., is useful to describe the behavior of lipid bilayers in which molecular shape determines a particular spontaneous curvature. For thin membranes, there is little energetic cost in bending compared to stretching, which is why edge growth gives rise to local buckling and wrinkles on the edge of some leaves.[52] Another example of the confluence of many of these concepts of differential geometry in a biophysical system is the opening of a chiral seed pod, where manipulation of various curvature parameters on two thin sheets stuck together yielded some stunning physical behavior.[53] This section aims to summarize how mechanics and biology are linked when morphologies develop to fulfill specific functions.

4.1. Molecular and Subcellular Scales

At the molecular level, the emergence of curvature is observed during the self-assembly of phospholipids (or glycolipids[54]) in polar liquids like water. Phospholipids constitute amphiphilic entities due to their hydrophilic head groups and hydrophobic tails. Hence, in the energetically most favorable states, head groups are exposed to the solvent while the tails are shielded. The properties and geometry of the amphiphilic lipids partly define the curvatures of the resulting structures. The simple view that individual lipid molecules have a specific shape leads to the concept of intrinsic lipid curvature.[6b,14b,c,55] Because they do not have an ideal cylindrical shape, lipids packed into a bilayer are frustrated[56] and because lipid bilayers can be considered fluid, lipid shapes depend on the immediate molecular environment. Thus, a relevant parameter describing bilayers curvature is the spontaneous (or preferred) curvature of the membrane, which reflects the asymmetry between the constituting leaflets and their immediate environment. The precise mechanisms of how molecule properties and concentrations can alter membrane curvature are manifold.[14a] Examples of how lipid leaflet asymmetry or the asymmetric insertion of partially water-soluble molecules can generate nonzero membrane spontaneous curvature are shown in **Figure 7**a. The generation of nonzero spontaneous curvature can be observed on model membranes such as giant vesicles, bilayer cell-sized structures allowing for direct microscopy interrogation.[57] Various membrane shapes might be found at an ultrastructural level, from simple sphere-like vesicles, tubules, or lamellar structures to more complex periodic conformations. Saddle points, which exhibit negative Gaussian curvature, may also appear when surface properties of a bilayer sheet are changed on both sides, e.g., in the presence of amphipathic peptides.[58] Under appropriate conditions, membranes can form shapes consisting of saddle points only. Prominent examples are cubic membranes, which are 3D nanostructures that correspond to mathematically well-defined triply-periodic minimal surfaces (zero mean curvature)[59] (see Section 2.1 and Figure 7b,c). They can self-organize from the plethora of membrane types (from the endoplasmic reticulum to plastid membranes) and are found in different organism species (from protozoa to mammals).[15,59a,60] Often, cubic membranes emerge where an increased amount of phospholipids or certain proteins are produced due to pathogenic alterations of the cell. Typical physiological examples of cubic membranes are the light-sensitive prolamellar body present in plant cell chloroplast precursor[61] and the inner membrane of starved amoeba mitochondria.[15] As such membranes make up the boundaries of cell organelles, they define the organelle shape and its inner organization, which is determined by its function. The endoplasmic reticulum and the Golgi apparatus are both designed to provide efficient protein trafficking and hence adopt a shape to maximize their surface area while keeping their volume low.[62]

The cubic folding of membranes is also a precursor for similar structures built up from other materials than amphiphilic lipids. For example, the gyroid-like morphology made of chitin in butterfly wings is proposed to be cast from the membrane of the endoplasmic reticulum, where the extracellular space is filled with chitin and remains as a solid network after the cells die and their cell compartments degrade.[63] These cubic structures lead to the colorful appearance of some butterflies (e.g., *Parides sesostris* or *Teinopalpus imperialis*) where, despite their chirality, they produce green reflections that are not circularly polarized.[63d,e,64] Although model lipid systems tend to form three-periodic minimal surfaces that divide space into two equivalent regions, in the biological examples mentioned above this balance can be lost and the surfaces are no longer minimal (see discussion in ref. [65]). However, these structures can still retain constant mean curvature but have different channel widths and represent material interfaces offset from minimal surfaces.[66]

4.2. Micro- and Macroscopic Scales

On the micro- and macroscopic scales, plants and animals developed a broad variety of strategies to form irregular, periodic, or self-similar shapes, which fulfil specific functions. Besides genetically programmed growth, simple physical principles are also exploited to create surface patterns, shapes, or dynamic materials.[3]
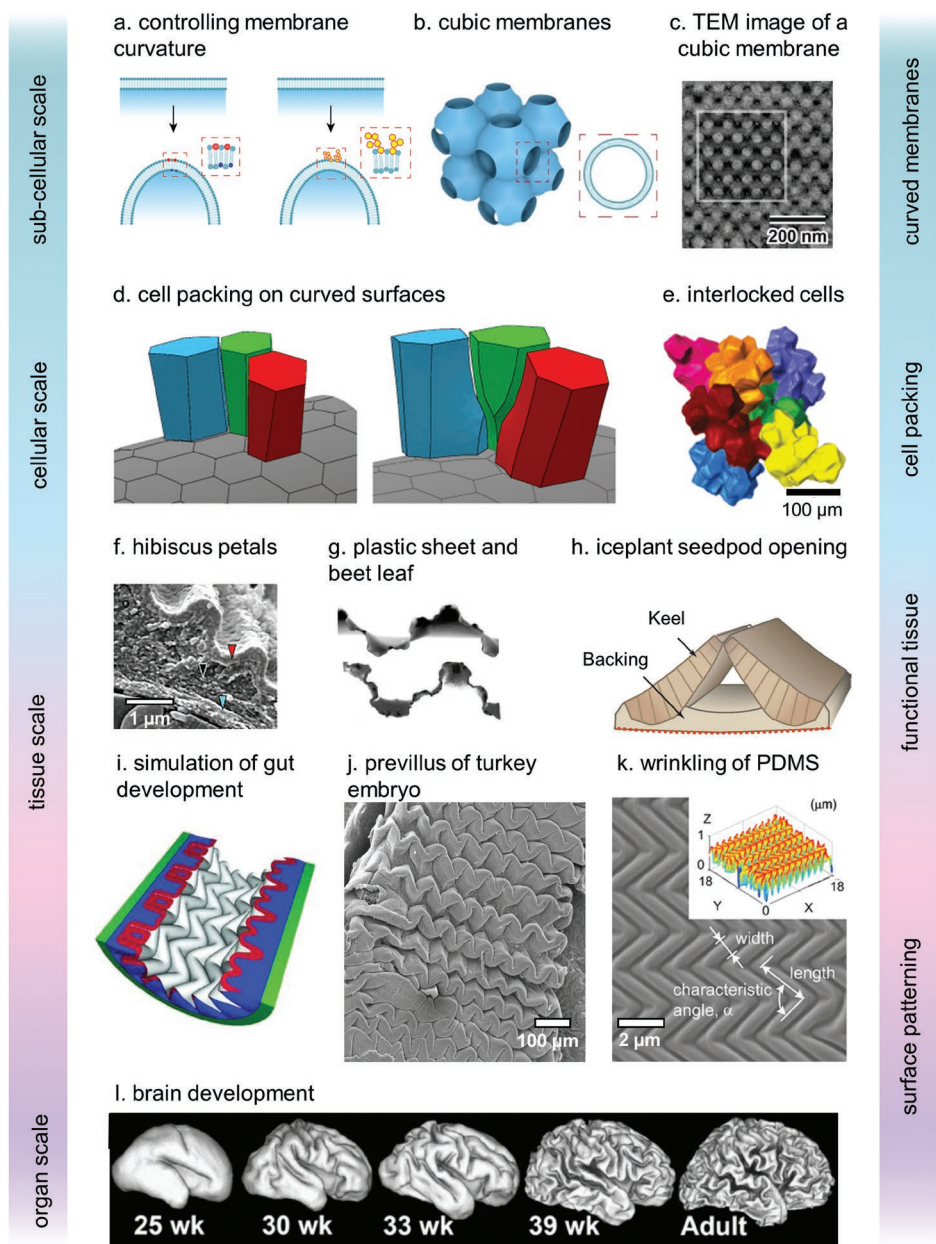
**ADVANCED
SCIENCE NEWS**

www.advancedsciencenews.com

**ADVANCED
MATERIALS**

www.advmat.de

Figure 7. Emergence of curvature on various length scales: a) Examples of sources generating nonzero spontaneous curvature in membranes: differences in the effective head-group size of the lipids or leaflet compositional asymmetry (left) or partially water-soluble molecules (such as glycolipids[36] or peripheral proteins[37]) asymmetrically inserting in or desorbing from the membrane (right). Adapted under the terms of the CC-BY Creative Commons Attribution 3.0 Unported license (https://creativecommons.org/licenses/by/3.0).[14a] Copyright 2018, IOP Publishing Ltd. b) Example of a cubic membrane formed by a lipid bilayer. c) Transmission electron microscope image of the cubic membrane of an etioplast (a plant cell organelle). Reproduced under the terms of the CC BY Creative Commons Attribution 4.0 International license (https://creativecommons.org/licenses/by/4.0).[10b] Copyright 2021, The Authors, published by Oxford University Press on behalf of American Society of Plant Biologists. d) Cell packing on 2D surfaces and in 3D: simulated shapes of tightly packed cells on curved surfaces of prisms with only hexagonal faces (left) and scutoid shapes (middle). Reproduced with permission.[38] Copyright 2018, Informa UK Limited, trading as Taylor & Francis Group. e) Segmentation of interlocked jigsaw puzzle-like cells in the walnut shell. Reproduced under the terms of the CC BY 4.0 license.[39] Copyright 2019, The Authors, published by Wiley-VCH. f) Cryo-SEM image of the fracture site of a hibiscus petal. The arrows indicate layers with different mechanical properties causing an optically active wrinkling pattern. Reproduced with permission.[40] Copyright 2021, Elsevier. g) Self-similar shape due to buckling of a torn and released plastic sheet (top) and beet leaf (bottom). Reproduced with permission.[41] Copyright 2002, Springer Nature. h) Scheme of the opening mechanisms of an ice plant seedpod in the closed (dry) state. Reproduced with permission.[42] Copyright 2011, Springer Nature. i) Simulation of pattern formation in chick gut lumen. Reproduced with permission.[43] Copyright 2013, AAAS. j) Zigzag pattern of previllus ridges of turkey embryos. Reproduced with permission.[44] Copyright 2013, The Authors, published by National Academy of Sciences, USA. k) Surface wrinkling after bidirectional stretching, plasma treatment, and releasing of a PDMS membrane. Reproduced with permission.[45] Copyright 2007, American Institute of Physics. l) Surface wrinkling of the human brain at different ages, indicated as weeks (wk). Reproduced with permission.[46] Copyright 2009, International Pediatrics Research Foundation, Inc.

2206110 (10 of 23)

**ADVANCED
SCIENCE NEWS**

www.advancedsciencenews.com

**ADVANCED
MATERIALS**

www.advmat.de

4.2.1. Bending- and Buckling-Induced Morphogenesis

Bending and buckling are the two main processes that transform a flat 2D layer into a curved 3D structure. These processes are exploited by plants and animals to create specific shapes with the help of basic physical principles. The observation that similar concepts are employed in a wide range of organisms highlights the fundamental character of these principles on morphogenesis across all kinds of live forms and length scales. Hence, we want to present selected examples from very different biological systems to discuss the emerging functionalities.

Bending mostly occurs in cell sheets like epithelia, where differences in contractility between surfaces of a cell create a bending moment that causes the folding of the tissue layer.[67] For instance, an increase in contractility of the apical surface drives Drosophila mesoderm invagination,[68] vertebrate lens placode invagination,[69] and folding of the intestinal crypt.[70] Conversely, an increase in basal tension generates curvature of opposite sign, as observed during the formation of the midbrain–hindbrain boundary folds and the optic cup in zebrafish.[71] Epithelial bending can also arise from a decrease (rather than an increase) in tension in one specific cell surface as observed during folding of the Drosophila wing disk.[72] Changes in contractility in lateral cellular surfaces have also been shown to play a role in epithelial bending during gastrulation in Drosophila[72] and in ascidians.[73] The patterns of contractility that give rise to bending are often complex, involving activation levels that differ within and between cell surfaces.[74] Buckling happens when an in-plane compression causes an out-of-plane movement in thin rods or sheets.[41] This is the case when the compression energy is distinctly larger than the bending energy at similar displacements of the boundaries.[75] In nature, tissue layers are often connected to a substrate, i.e., a thicker layer with different mechanical properties. Depending on the properties of the layers (e.g., Young's moduli, adhesion to the substrate)[76] and by introducing in-plane mechanical mismatch strain, a single buckle or multiple wrinkles may occur. Typical wrinkles form periodic wavy patterns with wavelengths and amplitudes depending on the ratio of Young's moduli, the Poisson's ratios, and the thickness of the tissue layer.[75] Single-layer systems can also develop 3D shapes through buckling. For example, beet leaves present remarkable similarities between their outer edge, where deformation may be induced by heterogenous cell growth/division rates (Figure 7g, lower panel), and the edge of a torn plastic sheet, where plastic deformation occurs during pulling while regions further away from the edge are deformed elastically (Figure 7g, upper panel).[41] The edges of both sheets exhibit a self-similar shape with the same wavy pattern, suggesting that the beet leave shape is due to the restricted boundary conditions. Although the biological functions of the wrinkled leave edges are not fully understood, thermoregulatory implications, as well as the increased mechanical stability, are likely advantageous.[77]

Bending and buckling can significantly increase the surface area within a confined space. Numerous examples are found in tissue development of higher organisms, where this process plays a pivotal role like in the formation of the outermost brain layer (cerebral cortex) of large mammals,[78] the shaping of lung's epithelium and glands, and much more.[79] Despite their different functions, the brain and intestine exhibit remarkable similarities during prenatal development. In both cases, large surfaces are crucial for the organ function for optimizing the area accessible by neurons or facilitating nutriment uptake. Differential or heterogenous growth rates are thought to cause mechanical instabilities triggering buckling events that significantly increase the surface-to-volume-ratio, followed by biological responses (Figure 7i–l).[44,78,80] The observation that early brain folding occurs at the same time as neuron differentiation suggests a causal link between the development of the brain's surface wrinkles (so-called gyri) and cell-biological processes. In the review,[78] it is concluded that the key to gyri formation might be an increased radial tissue growth rate in high-stress regions, thus amplifying geometric heterogeneities on the cortex surface. A comparable concept is suggested for the chicken intestine development, where anisotropic growth rates within different layers of the duodenum wall cause elastic stresses inside the tissue and form the mesenchyme, an epithelium bilayer system.[44] These stresses shape the tissue into a 3D herringbone pattern with a wavelength of around 100 µm (Figure 7j,k).[43] Wrinkle shapes of the intestine can be mimicked by plasma-treating biaxially stretched polydimethylsiloxane (PDMS) membranes and subsequent release. The compressive forces on the plasma-stiffened surface layer cause bucking and wrinkle formation (Figure 7k).[81] Systematic studies showed that by changing mechanical parameters of a film bound to a substrate with different stiffnesses, a wide range of shapes and wrinkles can be obtained.[76] The similarities in physical models and biological wrinkle patterns suggest a common role of mechanical instabilities being an important driving force for the development of form in biology.[82] A similar wrinkling mechanism is found in the hibiscus petal that modulates its optical properties (Figure 7f).[40] Even earlier in embryonic development, compressive mechanical stress due to differential tissue growth is suggested to induce the very first buckling events in forming cranial flexure (bending of the neuronal tube prior to brain development) which then eventually twists rightward.[83] Together with the rotation of the heart loop, these processes are the first symmetry-breaking events in embryogenesis.[84] The connection between tissue growth and the emergence of chirality is an expanding topic addressed in the references.[85]

4.2.2. Cell Packing and Morphogenesis

The stiffness and thickness of a structure limit the ability for buckling without provoking material failure (e.g., under exceeding the compressive strength). The formation of a curved "thick" structure can be facilitated via special cell packing and/or the combination of two or more layers with different swelling behavior. Such multilayer systems are widely used by plants and may remain functional after the death of the organism.[86]

Shape-changing materials triggered by environmental conditions are found in plants and are often involved in seed-releasing mechanisms. *Bauhinia variegata* seedpods,

**ADVANCED
SCIENCE NEWS**

www.advancedsciencenews.com

**ADVANCED
MATERIALS**

www.advmat.de

e.g., exhibit a hygromorphic (shape change due to humidity changes) behavior: two initially flat pod-halves are bilayers, consisting of sclerenchymal tissue (thick-walled, dead cells) oriented with +45° and −45° to the longitudinal pod direction.[53] Upon drying, both layers shrink perpendicular to the fiber orientation, causing the valves to deform into two helices allowing seed release. Alternatively, seed release can be triggered upon water exposure. In ice plants (*Delosperma nakurense*) for instance, swelling of the cellulosic inner layer of an anisotropic honeycomb structure (hygroscopic keel) drives the reversible unfolding motion of the seed pod closing valves (Figure 7h).[42] An essential function of seed pod structures is the ability to "sense" the right time for successful seed dispersal and (later) germination. However, the optimal conditions for seed release depend on ecosystems and plant species and are for Bauhinia drying after maturity and rain for ice-plants that grow in dry environments. In some cases, such as in Banksias even more than one trigger is required: heat, often in the form of fire leads to slight opening of the seed pod. After rain exposure, opening progresses until seed release into a nutrient-rich environment with sufficient water content. Such multiple-step opening processes require more complex mechanisms.[87]

While differential swelling of bulk material may facilitate rapid curvature changes, geometric implications also need to be considered in static or semistatic cases, as the tight packing of thick cells along 3D geometries becomes complex. Because surfaces of tissues, organs, and functional units in animals and plants are usually curved; the cells forming the outermost layers, e.g., epithelial cells, represent a barrier to the surroundings and have to comply with distinct physical constraints defined by the shape. Until recently, it was assumed that a finite local curvature of an epithelium causes an area difference between one side of a cell compared to the other side, assuming that the cells would always have the same neighboring cells from their apical to their basal side.[88] New studies revealed an additional packing form of cells, the so-called scutoids, where the cells intercalate within the apico-basal axis (Figure 7d).[38,89] Scutoids can appear in any bent epithelial tissue depending on the anisotropy of the tissue curvature and are more frequently observed in tubular epithelia, where the curvature anisotropy is maximized (curvature is null along the longitudinal axis and (1/radius) along the transversal axis).[89] The emergence of such cells in purely surface-tension driven systems has been demonstrated.[38]

Beside simple polygon-faced cells, plant cells covering curved surfaces can also expand to big cells with lobes (convex areas) and indentations (concave areas) that interlock into a jigsaw-like puzzle (Figure 7e). Molecular mechanisms have been proposed for patterning and coordination of these intricate packings, but mechanical and/or geometric cues turn out to play a crucial role.[90] Lobe formation was recently explained by a two-step mechanism: 1) de-methylated pectin nanofilaments stiffen the cell wall at the future indent and lead to cell wall undulation,[91] 2) more microtubules and in turn, more cellulose fibrils align at the more stressed indent cell wall and slow down locally cell expansion.[91b,92] In nutshells, 3D puzzle tissues made of polylobate cells exhibit remarkable mechanical properties as crack propagation is hampered due to the highly curved shapes of the densely packed interlocked cells.[39,93]

5. Curvature Signals in Biology

The complexity of investigating interaction between cells/organisms with their surrounding matrix arises from the manifold mechanisms involved, including the influence of chemical, biophysical, mechanical, and geometrical cues summarized under the term "materiomics."[100] Geometrical cues include surface curvature that may emerge from mechanical and biological processes as described in Section 4. Importantly, curvature also acts as a fundamental signal from the physical environment that will greatly affect the behavior of biological systems from cells to tissues to populations of organisms.

It is difficult to investigate cell behavior and tissue growth in natural systems as a function of curvature not only because curvature itself is often determined by growth (e.g., in developing embryos), but also because of the technical challenges inherent to in situ imaging of 3D living objects (see Section 3). To decouple the causes and the consequences of curvature on biological systems, one can culture well-characterized cells onto artificial substrates with well-known chemical, mechanical, and geometrical properties at different length scales. For example, applying controlled curvature to cells and tissues has helped to elucidate fundamental principles of development and morphogenesis like curvature sensing and curvature guidance, which determine cytoskeletal organization,[7a] cell motility, proliferation and differentiation,[101] collective cell behavior,[7b] and tissue formation[7c] (see **Figure 8**). **Table 2** summarizes different manufacturing approaches used to apply controlled curvature to cells and tissues. Similar to what is already done for surface topography,[102] such strategies could be integrated into the high-throughput work flows of materiomics studies in order to add different scales of curvature in the catalog of material properties to account for in the holistic considerations of complex biological systems.[100]

5.1. Organelles Shape and Cell Motility

Cell morphology and motility are strongly influenced by the geometry of their substrate via mechanosensing, whereby biochemical processes shape the cell membrane and organize its cytoskeleton to match the mechanical constraints imposed by the surroundings (see glossary).

When grown on nanometric pillars, the plasma membrane of melanoma cells shapes highly concave regions, which reveal higher endocytotic activity (Figure 8a). Endocytic proteins such as clathrin and dynamin preferentially localize in regions of positive membrane curvature with a radius < 200 nm.[94] Osteosarcoma cells cultured on similar nanofeatures concentrate the formation of actin fibers in a curvature-dependent manner up to $1/200$ nm^{-1}.[134] Such localized phenomena at the cell membrane trigger signaling cascades[135] and result in significant architectural and functional changes at the cell level through the distribution of focal adhesions and the reorganization of the cytoskeleton (see glossary).[136]

Although cells are known to align into the direction of nanopatterned surfaces,[137] this does not always apply on curved surfaces. On flat or semicylindrical surfaces of mesoscopic
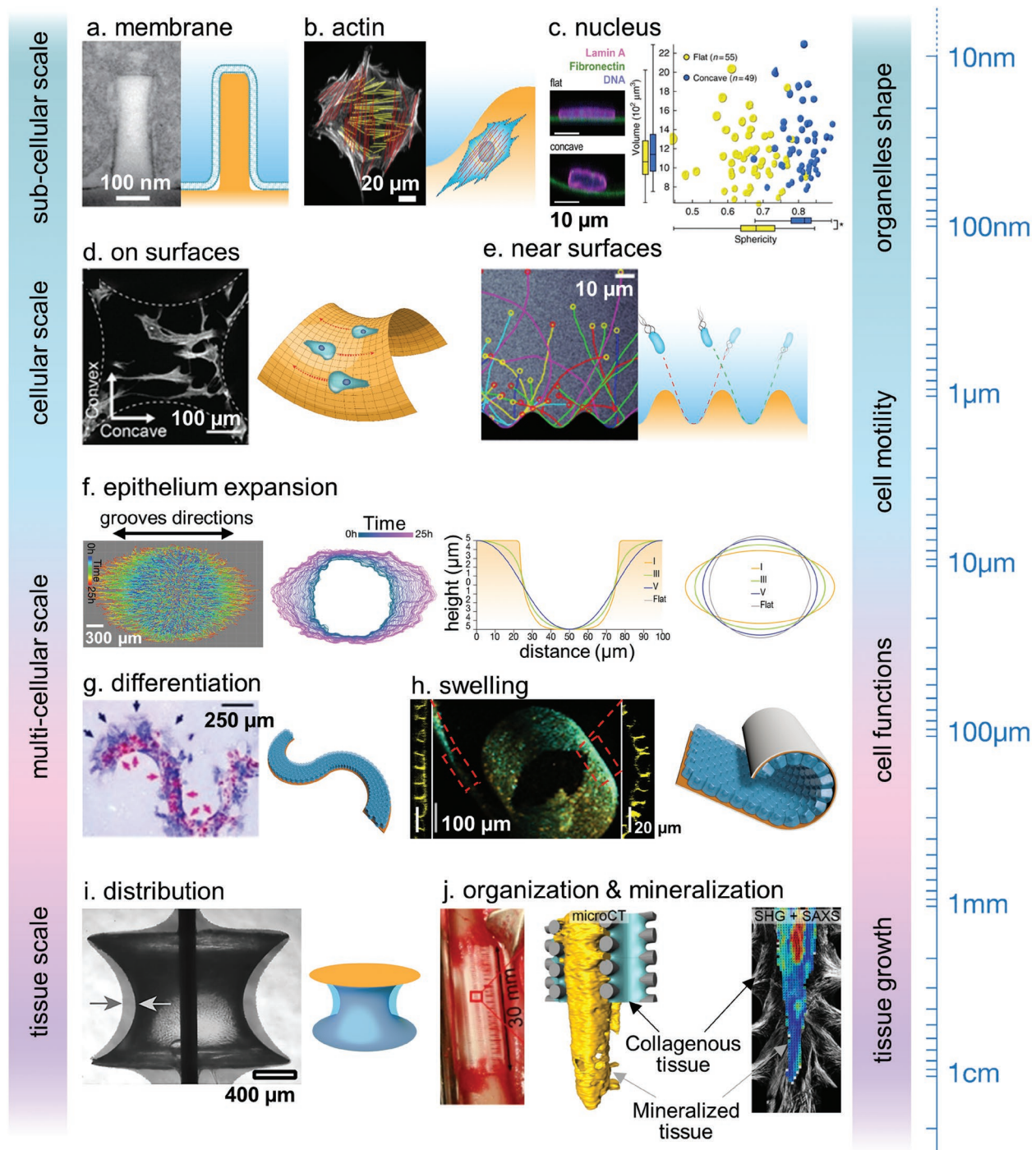
Figure 8. Effects of curvature on biological systems. a) Deformation by nanopillars of plasma membrane of melanoma cells. Reproduced with permission.[94] Copyright 2017, Springer Nature. b) Directional difference of apical and basal actin fibers in fibroblasts adhering on a cylinder. Reproduced with permission.[4c] Copyright 2018, Biophysical Society, published by Elsevier. c) Deformation of the nucleus of cells spread on concave or flat surfaces. Reproduced under the terms of the CC BY Creative Commons 4.0 International license (https://creativecommons.org/licenses/by/4.0).[4b] Copyright 2018, The Authors, published by Springer Nature. d) Migration of human bone marrow stromal cells on a saddle-shaped surface. Reproduced under the terms of the CC BY Creative Commons 4.0 International license (https://creativecommons.org/licenses/by/4.0).[4a] Copyright 2019, The Authors, published by Wiley-VCH. e) Movement of flagellated bacteria influenced by sidewall shape. Reproduced with permission.[95] Copyright 2019, American Physical Society. f) Epithelium elongation guided by topographical curvature. Reproduced under the terms of the CC BY Creative Commons 4.0 International license (https://creativecommons.org/licenses/by/4.0).[96] Copyright 2020, The Authors, published by Springer Nature. g) Spatial patterning of differentiation according to the curvature of the edges. Reproduced with permission.[97] Copyright 2008, Oxford University Press. h) Transient swelling of epithelial cells after induction of curvature of their substrate. i) Curvature-driven tissue growth on constant mean curvature surfaces. Reproduced with permission.[98] Copyright 2019, The Authors, published by AAAS. j) In vivo curvature-mediated mineralization of bone tissue. Reproduced with permission.[99] Copyright 2017, Acta Materialia Inc., published by Elsevier Ltd.

Table 2. Manufacturing surfaces with controlled curvatures.

Method	Principle	Applications/research question
2D surface patterning		
Microcontact printing	Transferring cell adhesive material to a surface using a prestructured soft stamp[103]	Cell shape morphology[104] Cell chirality[105]
Photopatterning	Selectively crosslinking or degrading photosensitive material with light exposure through a patterned mask	Tissue engineering[106] Biofilm engineering[107] Cytoskeletal organization in plant cells[108]
Nanoimprint lithography	Transfer of nm-sized structures in a polymer	Cell behavior on topological features (resolution <100 nm)[109]
Stencil micropatterning	Drawing shapes in a thin membrane using laser cutting[110]	Spatially organized cell differentiation[110b]
3D surface patterning		
Micromilling	Cutting out material with rotating tools[111]	Microfluidics for cell culture[111]
Doming	Patterning 2D surfaces for lumen formation[112]	Probing monolayer mechanics[112]
3D printing	Adding material layer by layer or stereo lithographic methods[113]	Tissue engineering[99]
Laser ablation	Melting or vaporizing material[114]	Tissue engineering[115]
Electrochemical manufacturing	Combining laser ablation and electrochemical etching[116]	Curvotaxis[4b,96] Bacterial attachment[117]
Molding and casting	Replicating structures Bioimprinting[118]	Investigation of cytoskeletal organization in mammalian[119] or plant cells[108] Cell migration[120] Cell adhesion[121]
Leveraging material stress		
Prestress	Stretching PDMS and stiffening its surface via plasma,[122] laser irradiation,[123] or generating a differential in-plane stress in a PDMS bilayer[124]	Response of epithelia cells to applied curvature (radius of curvature from tens to hundreds µm)[124] Bacterial attachment and biofilm growth[125]
Surface tension	Confining a droplet of resin to a restricted area to obtain defined surface curvature[98,126]	Curvature-driven tissue growth[98]
Morphodynamic surfaces		
Dynamic micropatterns	"Switch ON" or "Switch OFF" surface adhesiveness by, e.g., UV light[127] or electric stimulation[128]	Cell migration[127] Cell co-cultures[129]
Stress build-up & release	Inflating/deflating thin membranes (e.g., PDMS) to create a semi-sphere-like surface	Cell stretching, mechanosensing[130]
4D printing	Printing materials that change shape in a controlled way via an external stimulus like (pH or light)[131]	Tissue engineering[132]
Bioprinting	Printing bioinks made of cells or bacteria diluted in hydrogels to print 3D living materials[133]	Fabrication of adapting or self-healing products[133]

dimension which are coated with collagen fibrils, cells co-align with the collagen when the surface is flat whereas they increasingly prefer to align in the direction of zero-mean curvature (i.e., along the axis) on semicylinders of increasing curvature, despite collagen patterning in the perpendicular direction. An increase in phosphorylated myosin light chain levels was observed with increasing substrate curvature.[138] Interestingly, similar cells seeded on convex cylindrical substrates migrate more persistently along the axis (i.e., in the direction of zero-mean curvature) compared to cells seeded on concave cylindrical substrates.[4a] Understanding cell alignment and migration thus requires considering substrate geometry on various length scales.

More recently, fibroblasts cultured on mesoscopic cylinders revealed that substrate curvature guides actin fiber orientation and that basal actin fibers rather align circumferentially around the cylinder while apical actin fibers preferably align in the axial direction.[4,139] Consistently, fibroblasts sitting on surfaces with negative Gaussian curvature (e.g., saddle shape) align their basal actin fibers in the convex direction and their apical actin fibers in the concave direction (Figure 8b).[4c] Studies performed on surfaces with both principal curvatures adopting positive and/or negative values also reveal complex migration behavior mediated by cell cytoskeletal organization. For instance, human bone marrow stromal cells seeded on saddle-shaped surfaces migrate preferentially along the concave direction (Figure 8d).[4a] Also, mouse fibroblasts[140] and human mesenchymal stem cells (hMSCs)[141] grown on flat surfaces and concave or convex microwells, show higher migration velocities on concave surfaces while tending to move toward flat areas. The effective contact area between the cells and their substrate can explain these differences as the numerous focal adhesions on convex or flat substrates may slow down cell migration, while the partial lift up of the contractile cell from the concave

2206110 (14 of 23)

surfaces may facilitate crawling with long dendritic contractile extensions.[141] On sinusoidal surfaces, however, stem cells preferentially settle in the concave valleys, where they do not lift from the surface although their focal adhesions are reduced and their mechanical tension increased compared to cells sitting on convex hills.[4b] Curvature-driven cell migration, also known as "curvotaxis," is proposed to result from the displacement of the nucleus toward the closest concave minimum to minimize mechanical stress. Importantly, several computational models can reproduce such experimental observations of single cell migration on various complex surfaces.[142] A recent study also reported Snx33, a curvature-sensing protein located at the leading edge of a cell membrane, as a determinant of actin-driven cell migration on curved surfaces.[143] Using serrated channels with curvature radii much smaller than the size of a cell, nonadhesive cells were also found to use small-scale topographical cues to propel themselves following a minimal model of active actomyosin flows on curved substrates.[144]

Curvature-driven cell behavior also involves the nucleus as a mechanotransducer, which experiences changes in cell shape through the transmission of mechanical deformations from the cell membrane to the nuclear membrane via different cytoskeletal filaments like actin, microtubule, or intermediate filaments (see glossary).[1a,145] Accordingly, the nucleus of cells sitting on convex or flat surfaces is less spherical due to the contractile forces that squeeze it between the actin network and the substrate (Figure 8).[4b,141]

In addition to cell migration on surfaces, movements of organisms through liquids are also strongly influenced by the curvature of surrounding rigid boundaries. For example, the accumulation of flagellated bacteria moving on a flat surface close to flat boundaries is higher than along concave sidewalls with a radius of 12 μm (Figure 8e).[95] It has also been revealed that microalgae prefer concave areas of a confined space.[146] A study using pillars of mesoscopic dimensions reported similar behavior, whereby the bacteria were trapped for a longer time around pillars with a higher radius.[147] It is important to note that surface colonization also depends indirectly on shape as the local curvature changes hydrodynamic flow gradients.[148] These observations highlight the potential of tuning the surface design of materials, which are prone to biofilm contamination and biofouling.

5.2. Coordination in Multicell Systems

How geometrical cues affect collective migration behavior in cell sheets has recently gained interest to clarify biological processes like wound healing and morphogenesis. When cells evolving on a surface are confluent, their mutual interactions balance the constraints imposed by the underlying substrate. 2D[149] and 3D[150] multicellular models exist, where cells are represented by interacting agents confined to a surface while physically interacting with their neighbors. In addition, vertex models allow for the modeling of more intricate cell interactions such as cell–cell adhesion and/or tension with active propulsion and friction on the substrate.[151] When applied on nonplanar surfaces, such models can predict curvature-dependent features like density fluctuations or the formation

of singularities like vortices, which help to further expand our understanding of the emergence of dynamic collective patterns on complex substrates.

On planar and fully adhesive substrates, monitoring how epithelial cell sheets fill in predesigned gaps of defined geometries has led to the conclusion that wound closure is curvature-dependent and relies on the mechanical interplay of cytoskeleton contraction and cooperative cell crawling.[152] The tensional state of the cells is an important cue that is transmitted up to the nucleus and determines cell behavior like cell migration, proliferation, differentiation, and protein expression. For example, multicellular cultures on adhesive patterns of different shapes combined with a finite element model of a contracting monolayer showed that epithelial cells proliferate more in regions of high tension, i.e., in concave corners.[153] Recently, epithelia cultured on flower-shaped adhesive islands revealed higher actin fiber polarization and actin flow toward the edge of the cell along concave borders and higher actin retrograde flow along convex borders.[154] The intercellular contractile actin network, which is built through mechanical links at cell–cell junctions, allows cells to collectively span the epithelium over nonadhesive areas along the concave borders. While a similar setup revealed that stem cells oriented along concave borders differentiate into adipocytes and cells lying along convex borders become osteoblasts (Figure 8g),[97] recent studies using controlled 3D substrates confirmed that convex surfaces promote osteogenic differentiation of hMSC.[141] In contrast, mouse calvaria cells cultured on ceramic surfaces shaped with different groove geometries revealed faster osteogenesis in the valleys compared to flat surfaces.[155] As cell differentiation is associated with the synthesis of functional and structural proteins, geometry turns out to be a determining cue during tissue development.[156]

On 3D sinusoid landscapes, individual cells position themselves in concave regions[4b] but collections of cells coordinate to reach favorable tensional states that allow them to colonize other regions.[157] In concavities, the oriented tension accumulated in the multicellular system often results in tissue detachment.[158] Similarly, epithelial cells grown on flat fibronectin-coated substrates with circular nonadhesive islands of various sizes were also observed to spontaneously depart from the surface and form domes of different radii of curvature.[112] Such bulging occurs as cells pump osmolytes thereby increasing the pressure under the dome, which in turn determines their curvature (Young–Laplace law). The potential of mesoscale curvature to guide epithelium during growth was recently demonstrated on wavy surfaces made of cell-scale grooves and ridges of different curvatures at the ridge/groove junctions (Figure 8f).[96] Such curvature-driven anisotropic growth is characterized by curvature-dependent nuclei exclusion from convex regions and by longitudinal actin stress fiber alignment. Confluent and nonexpanding epithelium monolayers studied on similar surfaces revealed curvature-dependent cellular and nuclear shapes as well as thicker epithelial zones in the valleys and thinner ones on the ridges.[5b] These observations agree with energy minimization arguments arising from the mechanics of apico-lateral tensions with an increased nuclear/cytoplasmic YAP ratio on convex curvatures but a decreased ratio on concave curvatures.[5b] As for single cells, such mechanical

**ADVANCED
SCIENCE NEWS**

www.advancedsciencenews.com

**ADVANCED
MATERIALS**

www.advmat.de

constraints transmitted to the nucleus explain downstream effects as a function of local curvature, such as YAP nuclear localization.[5b]

To approach the 3D reality of cell native environments, epithelial cell migration and epithelium formation were studied in microtubes or on cylindrical wires. In tubes with diameters between 25 and 75 μm, cell velocity and forward polarization increase with the diameter. The lower velocity observed in the tubes with higher concavity is due to disturbances induced by cell division.[159] While cells migrate slowly but collectively on wires of radii > 40 μm, the leading cells tend to detach from the sheet and migrate faster than the rest of the population on thinner wires.[160] This transition correlates with a change in actin organization. High curvatures induce a circumferential alignment of actin fibers at the basal plane of cells. Cell monolayers were also subjected to tortuous microchannels of different shapes, which demonstrated that turnings as well as their curvature influence cell morphology and collective migration behavior. Leader cells with concave-shaped structure and actin bundles rearrangement in an orientation perpendicular to the free cell edge were observed leading the migration inside those tortuous microchannels.[161] Similarly, epithelial tissue growth performed in bent mesoscopic tubes mimicking native geometries showed that increased curvature leads to the local detachment of the cell layer and extrusion of cells from the epithelium due to the resulting forces on the tissue.[162] Interestingly, it was found using two types of renal epithelial cells, that cellular architecture on curved substrates was closely related to cell type-specific characteristics such as stiffness or cell–cell adherence.[163] Moreover, self-rolling substrates designed to investigate the understudied effects of shape change, revealed that the epithelium responds to rapid and anisotropic changes of curvature through a transient active osmotic swelling of the cells associated with a decrease in membrane tension and actin depolymerization (Figure 8h).[124] While this response was independent of the sign of the curvature, it was not observed on substrates with induced wrinkles where convex and concave regions alternate on short length scales. Adaptation to persistent curvature induction was concluded to result from a collective response of the epithelial cells. Whole-tissue collective epithelial rotation (CeR) plays a critical role in embryonic development and glandular tissue formation. A significant example of CeR is the follicle epithelial cell rotation around egg chamber during drosophila oogenesis.[164] A recent dynamic study of CeR using concave and convex cylindrical substrates confirmed that the circumferential epithelial rotation was similar on those substrates regardless of different actomyosin networks, cell–cell junction organization, and apico-basal polarity. However, stable cell–cell adhesions and Rac-1-dependent polarity were shown to be essential for lamellipodial protrusion formation and force transmission for persistent CeR.[165] Inspired by the spherical geometries found in lungs, recent work compared the behavior of epithelial cell sheets cultured on artificial hemispherical substrates (3D surfaces) and pluripotent stem cells (iPSCs) spontaneously forming alveolospheres in 3D Matrigel. Both approaches revealed that higher curvatures promote higher dynamics and more heterogeneity in multicellular flow fields.[166]

5.3. Tissue Growth and Architecture

Morphogenesis also involves the production and organization of ECM at larger scales. Historically, connective tissues making the musculo-skeletal system have been largely investigated in that respect.[167] In particular, multiple research groups motivated by tissue engineering perspectives have been focusing on bone morphogenesis and the environmental cues determining bone modeling and remodeling. In that context, studies of preosteoblasts growing in straight-sided pores of different geometries revealed that curvature is a key predictor for bone tissue growth.[168] Similar studies performed with other cell types (e.g., fibroblasts and bone marrow stromal cells) enabled to generalize and show that the rates of cell proliferation and matrix deposition (e.g., fibronectin and collagen) increase with decreasing pore diameter, i.e., increasing curvature.[169] In prismatic pores, local tissue growth rates are higher in concave corners compared to flat areas,[170] while cell densities are lower, as cells tend to elongate more with increasing curvature.[159] Interestingly, the architecture of the fibrous matrix bears the internal mechanical stresses, which were originally born by the contractile cells and shape the tissue.[171] Constraining the distribution of these stresses in the tissue using curved substrates also results in patterns of differentiation, e.g., from fibroblasts to myofibroblasts.[5a] To study tissue growth on negative Gaussian curvature surfaces where both concave and convex directions are found, preosteoblast cells were grown on capillary bridges of constant mean curvature.[98,126] Tissue growth increased with increasing mean curvature of the surface while reflecting the morphing behavior of a liquid (Figure 8i).[98] This observation highlights the relevance of using physical models to understand biological processes, as well as the importance of reliable shape measurements (described in Section 3) and a mathematical framework for quantitative curvature descriptions (described in Section 2).

Despite the significant potential of simple physical models in view of applications, further studies remain necessary to evaluate the contribution of additional factors present in physiological conditions. For example, more complex in vitro models involve perfusion systems to consider fluid flow, either for stimulating cells mechanically or for providing nutrients throughout a 3D construct. These aspects are especially important in the field of bone regeneration,[172] where scaffolds are now designed to both fulfil their mechanical function and support the biological activities driving tissue regeneration. Coupling scaffold geometry and fluid flow in tissue growth models has shown to improve the distribution of engineered tissue throughout the scaffolds,[173] while in silico systematic investigations revealed a critical role of the interplay between curvature-driven tissue growth and either flow stimulation or flow inhibition.[174] A significant effect of fluid flow on the amount and the morphology of mineralized tissue obtained in 3D scaffolds was also observed within channels of different sizes and shapes.[175]

Additional steps toward the translation of curvature-driven tissue growth and organization to the clinics rely on in vivo studies, which greatly benefit from the increasing capabilities of 3D printing.[132] Here again, bone tissue engineers and orthopedists have paved the way to study the role of scaffold

geometry in clinical contexts. For instance, layered 3D scaffolds printed with a fiber laydown pattern of 0°/60°/120° implanted in cranial defects induce less bone formation and weaker biomechanical properties compared to cross-like 0°/90° pattern.[176] Similarly, the tissue architecture obtained after implantation of 0°/90° scaffolds in sheep tibia, reveal an unusual biomineralization process that involved i) curvature-driven growth of soft tissue along the scaffold, ii) the formation of mineralized cones in the center of the pores, and iii) a continuous transition between these two phases (Figure 8j).[99] Another recent in vivo work for which the architecture of 3D printed scaffolds was systematically varied suggested that a 0°/45° strut geometry with larger pores promote osteointegration and vascularization in rat spine and enhance the chances of spinal fusion.[177]

Overall, the state-of-the-art spanning in silico, in vitro and in vivo work reveals that curvature is an underestimated descriptor of scaffold morphology and determinant of the subsequent engineered tissue architecture and function. When developing engineered tissues as clinical modalities, curvature should thus be considered as a critical process parameter and incorporated in the design of clinical implants early on. Building on the experimental data reviewed here and using mathematical concepts detailed in Section 2, in silico models of tissue growth allow integration of various aspects of scaffold design and to screen complex geometries numerically prior to their in vitro or in vivo testing.[99,178] For example, model-optimized 3D-printed hydroxyapatite-based gyroid scaffolds used in a maxillofacial orthotopic rat model recently proved to promote bone formation and penetration into the scaffold, compared to the clinical gold standard or 3D-printed orthogonal lattice structures.[179] Different methods used to model tissue growth have been reviewed in ref. [180]. Irrespective of the modeling approach, the final morphology of the object heavily depends on multiple parameters, including the boundary conditions of the system. Varying these parameters in silico is a powerful method to predict the tissue engineering performances of scaffolds,[181] especially if nutrient gradients, fluid flow, or cell differentiation are included to broaden the physiological relevance of the model.[174,182]

6. Curvature Feedback across Scales

In the previous sections, two main concepts describing how curvature interacts with biological systems have been addressed. First, there are systems where curvature is an emergent property of a growth process, such as in a hyperbolic leaf shape or a self-assembly process, such as those that lead to curved membranes. Second, there are biological processes that occur on curved surfaces, where the curvature of the surface influences a biological process, such as cell migration or filament growth. Of course, in vivo, there is likely a combination of the two perspectives, where surfaces are influencing biological processes occurring on them and in turn are being changed by those processes. The present section highlights how both the emergence of curvature (Section 4) and the effects of curvature on biological systems (Section 5) contribute to a cross-talk, which is mediated by passive and active transport phenomena, themselves influenced by spatial modifications inherent to

curvature changes (section 2). This complex curvature-feedback during morphogenesis is thus a key mechanism that controls the development of shapes at different scales (**Figure 9**).

One important aspect of morphogenesis is the control of the distribution of morphogens, signaling molecules that are known to modulate local growth processes (Figure 9a).[184] Morphogens have been identified as key players in pattern formation in various species. For example, the spacing between the hair follicles characterizing highly keratinized epidermis structures in mammals is due to the counter play of a morphogen, which initiates the formation of hair follicles and its inhibitor. The inhibitor secretion is directly linked to the morphogen secretion and therefore prevents follicle formation in the interfollicular space.[185] Similar mechanisms occur in birds in the form of feathers[186] and in reptiles in the form of scales.[187] Work going back to Turing[188] has shown that the spatial distribution of these morphogens is controlled by coupled processes of reaction and diffusion, leading to complex pattern formation. Although the diffusion rates of the morphogens, their reactivity, and ability to trigger a biological response are key factors in pattern formation,[188,189] geometric factors such as curvature may also modulate morphogen transport and thus the patterns formed.[156] For example, changes in Gaussian curvature due to localized growth, bending, or buckling of a surface can change the traveling distance and local density of diffusing morphogens confined within the surface.[190] Numerical studies also indicate that diffusion is much slower on highly curved membranes.[191] When discussing signal gradients, it is therefore important to consider the geometric constraints on transport of morphogens and specifically to distinguish between 3D and curved 2D systems. Although having a 3D shape, an epithelial monolayer forming a cyst is essentially 2D, since spatial patterning can only occur within the surface of the tissue. However, during embryonic development, signaling receptors are polarized entirely to one specific side of the tissue (the basal side of the epiblast).[192] Pattern formation can also be modulated by mechanical stress fields, with one example being the formation of scales on crocodiles' heads.[193] Stress concentrations due to the slower growth of the thick and highly keratinized skin compared to the underlying tissue lead to surface cracking. This pattern is in turn influenced by the presence of highly curved regions containing high concentrations of dome-pressure receptors used for orientation.[193]

Pattern formation is not just a macroscopic phenomenon and can occur at sub-cellular scales.[194] In epithelial tubes of the *Drosophila* trachea, actin bundles align in the form of periodic rings. It was shown that such rings result from an interplay of myosin activity, actin polymerization, and contraction-induced flow of myosin within a cell. Dilatation of the tube leads to instabilities in myosin distribution, which result in a locally changed actin turnover and formation of stable rings due to the interplay between actin and myosin.[195]

One tissue in which curvature may be of particular relevance in regulating cell function is the mammalian intestinal epithelium (Figure 9b,d). This tissue self-renews every 3–5 days thanks to the continuous division of stem cells located at the base of highly curved invaginations called crypts.[196] Cells progressively differentiate as they leave the crypt and migrate along the surface of finger-like protrusions called villi. Upon
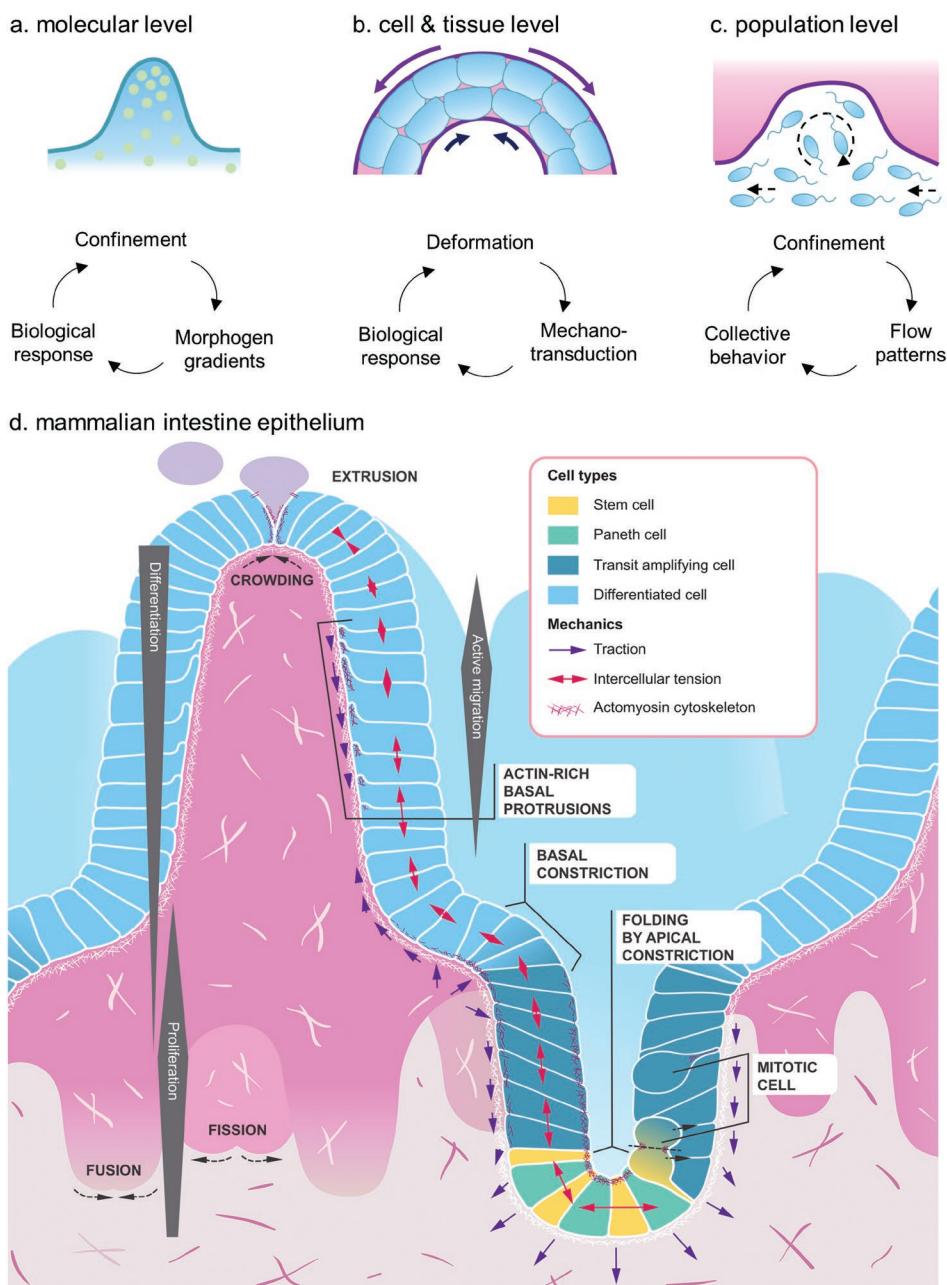
**ADVANCED
SCIENCE NEWS**

www.advancedsciencenews.com

**ADVANCED
MATERIALS**

www.advmat.de

Figure 9. Curvature feedback mechanisms at different length scales: a) Molecular level, b) cell and tissue level or c) population level. Curvature changes can either modulate the confinement of motile morphogenetic agents or of micro-organisms, or change the mechanical state of cells, leading to biological responses, which in turn change curvature. d) Example of intestinal epithelium. Adapted with permission.[183] Copyright 2021, The Authors, published by Elsevier.

reaching the tip of the villus, cells are extruded into the intestinal lumen. Villi and crypt show opposite curvature and they form at different developmental stages and through different mechanisms. Villi fold during embryonic development through buckling morphogenesis.[43,44] This leads to a local increase of the epithelial morphogen sonic hedgehog (Shh), while proliferating intestinal stem cell progenitors progressively localize into clusters at the base of the villi.[197] High levels of Shh signals then induce reciprocal signaling by bone morphogenetic pro-

teins within the cluster, repressing intestinal stem cell identity in the overlying epithelium and restricting stem cell proliferation to the base of the villi. During this process, fibroblasts and smooth muscle contract to drive folding of the ECM and the overlying epithelium. By contrast, the crypt forms postnatally through bending morphogenesis, a process that is well reproduced by intestinal organoids.[198] Recent experiments in these systems show that organoid progenitor monolayers develop spontaneous stem cell foci that progressively accumulate actin

and myosin at their apical surfaces.[70,199] Actomyosin contraction then creates a bending moment that pushes the stem cell niche toward the ECM and drives its folding. Throughout the life of the organism, stem cells remain segregated at the base of the crypt, where curvature is highest, but the extent to which there is a feedback between curvature and stemness remains unclear. When organoid monolayers are grown on surfaces with a curved pattern, stem cells tend to localize highly curved crypt-like structures.[200] However, stemness and segregation are retained when organoids are grown on flat surfaces.[70,201] The link between curvature, fate, and function in the intestinal epithelium is thus a major open question.

Micro-organisms populate the complex and dynamic environments of our daily lives and when viewed as a collective can even be considered as a class of microscaled active matter (Figure 9c). Geometry, topology (as defined in Section 2), and flow—the primary descriptors of microbial environments—play a critical role in determining their physiology and behavior, thereby regulating the health and resilience of the ecosystems made of micro-organisms. An active interplay between curvature and microbial activity triggers has been shown to induce dynamical patterns, thereby eliciting novel transitions with time-dependent characteristics.[202] The long-range orientational and positional correlations in active living systems nucleate disordered hotspots known as topological defects, which arise due to spontaneous symmetry breaking in an ordered field.[203] Confluent microbial colonies containing rod-like organisms may behave similarly to active nematic liquid crystals giving rise to anisotropic stresses and hydrodynamic fields,[204] which of course will couple to the shape and curvature of the surrounding environment.[205]

7. Conclusion

Nature uses a wide range of tools involving biological, physical, and biochemical mechanisms to generate complex shapes and to facilitate regulated tissue growth. This article has reviewed the current state of the art of how curvature acts as a key feature in morphogenesis. We see that curvature is not only a result of morphogenesis but also a signal, inducing biophysical responses and triggering further morphological processes. This gives rise to feedback loops within the biological entities on length scales spanning from the membrane level up to whole organisms. To gain a comprehensive picture of morphogenesis requires bringing together mathematicians, biologists, biochemists, physicists, and engineers and refine the common language to bridge and connect the different fields. This review is the result of the ambitious attempt to do this by involving numerous experts from different disciplines. It gives an insight into the mathematical background of differential geometry, the possible ways of quantifying curvature of surfaces, how mechanosensing of cells works as well as potential use of theoretical modeling techniques.

This highly interdisciplinary emerging research field provides numerous challenges for the upcoming years. From a mathematical point of view, the theoretical understanding of describing and measuring 3D curvature based on discrete datasets as they are obtained in physical experiments is still

ongoing research. Establishing standardized curvature measures will help for the translation to the biological world and provide better comparison between studies. The possibility to design scaffolds with mathematically defined geometries rapidly increases with the technological advances of manufacturing techniques, but still the demand for smooth or patterned 3D scaffolds with specific surface properties and shapes is often limited by feasibility and costs. The investigation of biological systems in interaction with such predefined shapes, can teach us about the fundamental principles that nature uses to connect the physical and the biological worlds. Much of the research exploring the role of curvature in biological systems has been done on mammalian cells motivated by medical applications, and the choice of examples in this review reflects this. This being said, we believe that many of the mechanisms behind curvature development and sensing are valid across multiple phyla and kingdoms. The wide range of potential biological model systems, experimental geometries, and conditions requires an extensive exchange between the researchers and an active community to guarantee the necessary knowledge transfer. We feel that this relatively young research field has a big potential to become an established discipline that complements mechanobiology and brings the focus into geometrical aspects.

Conflict of Interest

The authors declare no conflict of interest.

**ADVANCED
SCIENCE NEWS**

www.advancedsciencenews.com

**ADVANCED
MATERIALS**

www.advmat.de

[1] a) K. Anselme, N. T. Wakhloo, P. Rougerie, L. Pieuchot, *Adv. Health-care Mater.* **2018**, *7*, 1701154; b) G. R. Fedorchak, A. Kaminski, J. Lammerding, *Prog. Biophys. Mol. Biol.* **2014**, *115*, 76.

[2] I. Schoen, B. L. Pruitt, V. Vogel, *Annu. Rev. Mater. Res.* **2013**, *43*, 589.

[3] D. A. W. Thompson, *On Growth and Form*, Cambridge University Press, Cambridge, UK **1992**.

[4] a) M. Werner, A. Petersen, N. A. Kurniawan, C. V. C. Bouten, *Adv. Biosyst.* **2019**, *3*, 1900080; b) L. Pieuchot, J. Marteau, A. Guignandon, T. Dos Santos, I. Brigaud, P.-F. Chauvy, T. Cloatre, A. Ponche, T. Petithory, P. Rougerie, M. Vassaux, J.-L. Milan, N. Tusamda Wakhloo, A. Spangenberg, M. Bigerelle, K. Anselme, *Nat. Commun.* **2018**, *9*, 3995; c) N. D. Bade, T. Xu, R. D. Kamien, R. K. Assoian, K. J. Stebe, *Biophys. J.* **2018**, *114*, 1467.

[5] a) P. Kollmannsberger, C. M. Bidan, J. W. C. Dunlop, P. Fratzl, V. Vogel, *Sci. Adv.* **2018**, *4*, eaao4881; b) M. Luciano, S.-L. Xue, W. H. De Vos, L. Redondo-Morata, M. Surin, F. Lafont, E. Hannezo, S. Gabriele, *Nat. Phys.* **2021**, *17*, 1382.

[6] a) I. K. Jarsch, F. Daste, J. L. Gallop, *J. Cell Biol.* **2016**, *214*, 375; b) S. Hyde, S. Andersson, K. Larsson, Z. Blum, T. Landh, S. Lidin, B. Ninham, *The Language of Shape: The Role of Curvature in Condensed Matter: Physics, Chemistry and Biology*, Elsevier Science, New York **1997**; c) R. D. Kamien, *Rev. Mod. Phys.* **2002**, *74*, 953.

[7] a) R. K. Assoian, N. D. Bade, C. V. Cameron, K. J. Stebe, *Open Biol.* **2019**, *9*, 190155; b) D. Baptista, L. Teixeira, C. van Blitters wijk, S. Giselbrecht, R. Truckenmüller, *Trends Biotechnol.* **2019**, *37*, 838; c) S. J. Callens, R. J. Uyttendaele, L. E. Fratila-Apachitei, A. A. Zadpoor, *Biomaterials* **2020**, *232*, 119739.

[8] B. Li, Y.-P. Cao, X.-Q. Feng, H. Gao, *Soft Matter* **2012**, *8*, 5728.

[9] a) S. J. P. Callens, D. C. Tourolle né Betts, R. Müller, A. A. Zadpoor, *Acta Biomater.* **2021**, *130*, 343; b) M. Kronenberger, O. Wirjadi, H. Hagen, *IEEE Trans. Visualization Comput. Graphics* **2018**, *25*, 3032; c) G. E. Schröder-Turk, W. Mickel, S. C. Kapfer, F. M. Schaller, B. Breidenbach, D. Hug, K. Mecke, *New J. Phys.* **2013**, *15*, 083028.

[10] a) P. Barbier de Reuille, A.-L. Routier-Kierzkowska, D. Kierzkowski, G. W. Bassel, T. Schüpbach, G. Tauriello, N. Bajpai, S. Strauss, A. Weber, A. Kiss, A. Burian, H. Hofhuis, A. Sapala, M. Lipowczan, M. B. Heimlicher, S. Robinson, E. M. Bayer, K. Basler, P. Koumoutsakos, A. H. K. Roeder, T. Aegerter-Wilmsen, N. Nakayama, M. Tsiantis, A. Hay, D. Kwiatkowska, I. Xenarios, C. Kuhlemeier, R. S. Smith, *eLlife* **2015**, *4*, e05864; b) T. M. Hain, M. Bykowski, M. Saba, M. E. Evans, G. E. Schröder-Turk, Ł. Kowalewska, *Plant Physiol.* **2021**, *188*, 81.

[11] P. Jin, L. Y. Jan, Y.-N. Jan, *Annu. Rev. Neurosci.* **2020**, *43*, 207.

[12] C. Frantz, K. M. Stewart, V. M. Weaver, *J. Cell Sci.* **2010**, *123*, 4195.

[13] a) K. Crane, CS 15-458/858: Discrete Differential Geometry, https://brickisland.net/DDGSpring2019/2019/03/13/steiner-formula-for-surfaces-in-mathbbr3/ (accessed: March 2022).

[14] a) P. Bassereau, R. Jin, T. Baumgart, M. Deserno, R. Dimova, V. A. Frolov, P. V. Bashkirov, H. Grubmüller, R. Jahn, H. J. Risselada, *J. Phys. D: Appl. Phys.* **2018**, *51*, 343001; b) C. Tanford, *The Hydrophobic Effect: Formation of Micelles and Biological Membranes*, Wiley, New York **1973**; c) J. N. Israelachvili, D. J. Mitchell, B. W. Ninham, *J. Chem. Soc.* **1976**, *72*, 1525.

[15] Z. A. Almsherqi, T. Landh, S. D. Kohlwein, Y. R. Deng, *Int. Rev. Cell Mol. Biol.* **2009**, *274*, 275.

[16] M. E. Evans, G. E. Schröder-Turk, *Mitt. Dtsch. Math.-Ver.* **2014**, *22*, 158.

[17] M. P. do Carmo, *Differential Geometry of Curves and Surfaces*, Dover Publications Inc., Mineola, NY, USA **2016**.

[18] a) A. M. Turner, V. Vitelli, D. R. Nelson, *Rev. Mod. Phys.* **2010**, *82*, 1301; b) V. Vitelli, W. Irvine, *Soft Matter* **2013**, *9*, 8086; c) T. Lopez-Leon, V. Koning, K. B. S. Devaiah, V. Vitelli, A. Fernandez-Nieves, *Nat. Phys.* **2011**, *7*, 391.

[19] a) T. B. Saw, A. Doostmohammadi, V. Nier, L. Kocgozlu, S. Thampi, Y. Toyama, P. Marcq, C. T. Lim, J. M. Yeomans, B. Ladoux, *Nature* **2017**, *544*, 212; b) A. Sengupta, *Front. Phys.* **2020**, *8*, 184; c) P. Guillamat, C. Blanch-Mercader, G. Pernollet, K. Kruse, A. Roux, *Nat. Mater.* **2022**, *21*, 588.

[20] V. Kralj-Iglič, V. Heinrich, S. Svetina, B. Žekš, *Eur. Phys. J. E.: Soft Matter Biol. Phys.* **1999**, *10*, 5.

[21] K. Crane, *Discrete Differential Geometry: An Applied Introduction*, https://www.cs.cmu.edu/~kmcrane/Projects/DDG/ (accessed: February 2022).

[22] G. Dziuk, C. M. Elliott, *Acta Numer.* **2013**, *22*, 289.

[23] A. I. Bobenko, J. M. Sullivan, P. Schröder, G. Ziegler, *Discrete Differential Geometry*, Vol. 38, Springer, New York **2008**.

[24] P. Grohs, M. Holler, A. Weinmann, *Handbook of Variational Methods for Nonlinear Geometric Data*, Springer, New York **2020**.

[25] C. W. Sensen, B. Hallgrímsson, *Advanced Imaging in Biology and Medicine: Technology, Software Environments, Applications*, Springer Science & Business Media, New York **2008**.

[26] P. Grangeat, *Mathematical Framework of Cone Beam 3D Reconstruction Via the First Derivative of the Radon Transform*, (Eds.: G. T. Herman, A. K. Louis, F. Natterer), Mathematical Methods in Tomography, Lecture Notes in Mathematics, Springer, Berlin/Heidelberg, Germany **1991**, https://doi.org/10.1007/BFb0084509.

[27] S. Rusinkiewicz, *trimesh2*, https://gfx.cs.princeton.edu/proj/trimesh2/ (accessed: March 2020).

[28] M. Fisher, P. Schröder, M. Desbrun, H. Hoppe, *ACM Trans. Graphics* **2007**, *26*, 56.

[29] H. Pan, Y.-K. Choi, Y. Liu, W. Hu, Q. Du, K. Polthier, C. Zhang, W. Wang, *ACM Trans. Graphics* **2012**, *31*, 85.

[30] M. K. Driscoll, E. S. Welf, A. R. Jamieson, K. M. Dean, T. Isogai, R. Fiolka, G. Danuser, *Nat. Methods* **2019**, *16*, 1037.

[31] O. Monga, S. Benayoun, *Comput. Vision Image Understanding* **1995**, *61*, 171.

[32] O. Monga, R. Deriche, G. Malandain, J. P. Cocquerez, *Image Vision Comput.* **1991**, *9*, 203.

[33] J. Fouchard, T. P. J. Wyatt, A. Proag, A. Lisica, N. Khalilgharibi, P. Recho, M. Suzanne, A. Kabla, G. Charras, *Proc. Natl. Acad. Sci. USA* **2020**, *117*, 9377.

[34] K. Khairy, W. Lemon, F. Amat, P. J. Keller, *Biophys. J.* **2018**, *114*, 267.

[35] J. D. Hauenstein, T. S. Newman, *Comput. Graphics* **2020**, *86*, 52.

[36] R. Dasgupta, M. S. Miettinen, N. Fricke, R. Lipowsky, R. Dimova, *Proc. Natl. Acad. Sci. USA* **2018**, *115*, 5756.

[37] H. T. McMahon, J. L. Gallop, *Nature* **2005**, *438*, 590.

[38] A. Mughal, S. Cox, D. Weaire, S. Burke, S. Hutzler, *Philos. Mag. Lett.* **2018**, *98*, 358.

[39] S. J. Antreich, N. Xiao, J. C. Huss, N. Horbelt, M. Eder, R. Weinkamer, N. Gierlinger, *Adv. Sci.* **2019**, *6*, 1900644.

[40] C. A. Airoldi, C. A. Lugo, R. Wightman, B. J. Glover, S. Robinson, *Cell Rep.* **2021**, *36*, 109715.

[41] E. Sharon, B. Roman, M. Marder, G.-S. Shin, H. L. Swinney, *Nature* **2002**, *419*, 579.

[42] M. J. Harrington, K. Razghandi, F. Ditsch, L. Guiducci, M. Rueggeberg, J. W. C. Dunlop, P. Fratzl, C. Neinhuis, I. Burgert, *Nat. Commun.* **2011**, *2*, 337.

[43] A. E. Shyer, T. Tallinen, N. L. Nerurkar, Z. Wei, E. S. Gil, D. L. Kaplan, C. J. Tabin, L. Mahadevan, *Science* **2013**, *342*, 212.

[44] M. B. Amar, F. Jia, *Proc. Natl. Acad. Sci. USA* **2013**, *110*, 10525.

[45] P.-C. Lin, S. Yang, *Appl. Phys. Lett.* **2007**, *90*, 241903.

[46] A. R. Barnette, J. J. Neil, C. D. Kroenke, J. L. Griffith, A. A. Epstein, P. V. Bayly, A. K. Knutsen, T. E. Inder, *Pediatr. Res.* **2009**, *66*, 80.

[47] A. Goriely, M. G. D. Geers, G. A. Holzapfel, J. Jayamohan, A. Jérusalem, S. Sivaloganathan, W. Squier, J. A. W. van Dommelen, S. Waters, E. Kuhl, *Biomech. Model. Mechanobiol.* **2015**, *14*, 931.

[48] H. Ucar, S. Watanabe, J. Noguchi, Y. Morimoto, Y. Iino, S. Yagishita, H. Takahashi, H. Kasai, *Nature* **2021**, *600*, 686.

**ADVANCED
SCIENCE NEWS**

www.advancedsciencenews.com

**ADVANCED
MATERIALS**

www.advmat.de

[49] P. S. Laplace, *Traité de Mécanique Céleste*, Vol. 4, Crapelet, Paris, France **1805**.

[50] F. J. Almgren, J. E. Taylor, *Sci. Am.* **1976**, *235*, 82.

[51] R. Lipowsky, *Nature* **1991**, *349*, 475.

[52] A. Boudaoud, *Trends Plant Sci.* **2010**, *15*, 353.

[53] S. Armon, E. Efrati, R. Kupferman, E. Sharon, *Science* **2011**, *333*, 1726.

[54] K. Kobayashi, K. Endo, H. Wada, *Subcell. Biochem.* **2016**, *86*, 21.

[55] D. Marsh, *Biophys. J.* **1996**, *70*, 2248.

[56] J. F. Sadoc, J. Charvolin, *J. Phys. France* **1986**, *47*, 683.

[57] R. Dimova, C. Marques, *The Giant Vesicle Book*, CRC Press, Boca Raton, FL **2019**.

[58] R. Downing, G. V. Bossa, S. May, *Soft Matter* **2020**, *16*, 5032.

[59] a) Z. A. Almsherqi, S. D. Kohlwein, Y. Deng, *J. Cell Biol.* **2006**, *173*, 839; b) J. J. K. Kirkensgaard, M. E. Evans, L. de Campo, S. T. Hyde, *Proc. Natl. Acad. Sci. USA* **2014**, *111*, 1271.

[60] C. Cui, Y. Deng, L. Han, *Sci. China Mater.* **2020**, *63*, 686.

[61] a) B. E. S. Gunning, *Protoplasma* **1965**, *60*, 111; b) Ł. Kowalewska, R. Mazur, S. Suski, M. Garstka, A. Mostowska, *Plant Cell* **2016**, *28*, 875.

[62] J. Zimmerberg, M. M. Kozlov, *Nat. Rev. Mol. Cell Biol.* **2006**, *7*, 9.

[63] a) H. T. Ghiradella, M. W. Butler, *J. R. Soc., Interface* **2009**, *6*, S243; b) H. Ghiradella, *J. Morphol.* **1989**, *202*, 69; c) V. Saranathan, C. O. Osuji, S. G. Mochrie, H. Noh, S. Narayanan, A. Sandy, E. R. Dufresne, R. O. Prum, *Proc. Natl. Acad. Sci. USA* **2010**, *107*, 11676; d) K. Michielsen, D. Stavenga, *J. R. Soc., Interface* **2008**, *5*, 85; e) G. E. Schröder-Turk, S. Wickham, H. Averdunk, F. Brink, J. F. Gerald, L. Poladian, M. Large, S. Hyde, *J. Struct. Biol.* **2011**, *174*, 290.

[64] M. Saba, B. D. Wilts, J. Hielscher, G. E. Schröder-Turk, *Mater. Today: Proc.* **2014**, *1*, 193.

[65] G. E. Schröder-Turk, *Faraday Discuss.* **2020**, *223*, 307.

[66] K. Große-Brauckmann, *Exp. Math.* **1997**, *6*, 33.

[67] A. C. Martin, M. Gelbart, R. Fernandez-Gonzalez, M. Kaschube, E. F. Wieschaus, *J. Cell Biol.* **2010**, *188*, 735.

[68] D. Sweeton, S. Parks, M. Costa, E. Wieschaus, *Development* **1991**, *112*, 775.

[69] T. F. Plageman, Jr., B. K. Chauhan, C. Yang, F. Jaudon, X. Shang, Y. Zheng, M. Lou, A. Debant, J. D. Hildebrand, R. A. Lang, *Development* **2011**, *138*, 5177.

[70] C. Pérez-González, G. Ceada, F. Greco, M. Matejčić, M. Gómez-González, N. Castro, A. Menendez, S. Kale, D. Krndija, A. G. Clark, V. R. Gannavarapu, A. Álvarez-Varela, P. Roca-Cusachs, E. Batlle, D. M. Vignjevic, M. Arroyo, X. Trepat, *Nat. Cell Biol.* **2021**, *23*, 745.

[71] J. Sidhaye, C. Norden, *eLife* **2017**, *6*, e22689.

[72] L. Sui, S. Alt, M. Weigert, N. Dye, S. Eaton, F. Jug, E. W. Myers, F. Jülicher, G. Salbreux, C. Dahmann, *Nat. Commun.* **2018**, *9*, 4620.

[73] K. Sherrard, F. Robin, P. Lemaire, E. Munro, *Curr. Biol.* **2010**, *20*, 1499.

[74] D. N. Clarke, A. C. Martin, *Curr. Biol.* **2021**, *31*, R667.

[75] C. M. Nelson, *J. Biomech. Eng.* **2016**, *138*, 021005.

[76] Q. Wang, X. Zhao, *Sci. Rep.* **2015**, *5*, 8887.

[77] A. B. Nicotra, A. Leigh, C. K. Boyce, C. S. Jones, K. J. Niklas, D. L. Royer, H. Tsukaya, *Funct. Plant Biol.* **2011**, *38*, 535.

[78] P. V. Bayly, L. A. Taber, C. D. Kroenke, *J. Mech. Behav. Biomed. Mater.* **2014**, *29*, 568.

[79] a) Y. Tan, B. Hu, J. Song, Z. Chu, W. Wu, *Nano-Micro Lett.* **2020**, *12*, 101; b) R. J. Metzger, M. A. Krasnow, *Science* **1999**, *284*, 1635.

[80] a) A. Trushko, I. Di Meglio, A. Merzouki, C. Blanch-Mercader, S. Abuhattum, J. Guck, K. Alessandri, P. Nassoy, K. Kruse, B. Chopard, A. Roux, *Dev. Cell* **2020**, *54*, 655; b) I. Di Meglio, A. Trushko, P. Guillamat, C. Blanch-Mercader, S. Abuhattum, A. Roux, *Cell Rep.* **2022**, *40*, 111227.

[81] A. Schweikart, A. Fery, *Microchim. Acta* **2009**, *165*, 249.

[82] V. A. Surapaneni, M. Schindler, R. Ziege, L. C. de Faria, J. Wölfer, C. M. Bidan, F. H. Mollen, S. Amini, S. Hanna, M. N. Dean, *Integr. Comp. Biol.* **2022**, *62*, 749.

[83] T. Takamatsu, S. Fujita, *Dev., Growth Differ.* **1987**, *29*, 497.

[84] Z. Chen, Q. Guo, E. Dai, N. Forsch, L. A. Taber, *J. R. Soc., Interface* **2016**, *13*, 20160395.

[85] a) L. Q. Wan, A. S. Chin, K. E. Worley, P. Ray, *Philos. Trans. R. Soc. B: Biol. Sci.* **2016**, *371*, 20150413; b) A. S. Chin, K. E. Worley, P. Ray, G. Kaur, J. Fan, L. Q. Wan, *Proc. Natl. Acad. Sci. USA* **2018**, *115*, 12188; c) D. W. Green, J. M. Lee, E. J. Kim, D. J. Lee, H. S. Jung, *Adv. Mater. Interfaces* **2016**, *3*, 1500411; d) Y. Wang, J. Xu, Y. Wang, H. Chen, *Chem. Soc. Rev.* **2013**, *42*, 2930.

[86] M. Eder, W. Schäffner, I. Burgert, P. Fratzl, *Adv. Mater.* **2020**, *33*, 2001412.

[87] J. C. Huss, V. Schoeppler, D. J. Merritt, C. Best, E. Maire, J. Adrien, O. Spaeker, N. Janssen, J. Gladisch, N. Gierlinger, *Adv. Sci.* **2018**, *5*, 1700572.

[88] T. Lecuit, P.-F. Lenne, *Nat. Rev. Mol. Cell Biol.* **2007**, *8*, 633.

[89] P. Gómez-Gálvez, P. Vicente-Munuera, A. Tagua, C. Forja, A. M. Castro, M. Letrán, A. Valencia-Expósito, C. Grima, M. Bermúdez-Gallardo, Ó. Serrano-Pérez-Higueras, F. Cavodeassi, S. Sotillos, M. D. Martín-Bermudo, A. Márquez, J. Buceta, L. M. Escudero, *Nat. Commun.* **2018**, *9*, 2960.

[90] a) A. Sapala, A. Runions, A.-L. Routier-Kierzkowska, M. D. Gupta, L. Hong, H. Hofhuis, S. Verger, G. Mosca, C.-B. Li, A. Hay, *eLife* **2018**, *7*, e32794; b) W. Lin, Z. Yang, *Curr. Opin. Plant Biol.* **2020**, *57*, 142.

[91] a) M. Majda, P. Grones, I.-M. Sintorn, T. Vain, P. Milani, P. Krupinski, B. Zagórska-Marek, C. Viotti, H. Jönsson, E. J. Mellerowicz, O. Hamant, S. Robert, *Dev. Cell* **2017**, *43*, 290; b) B. Altartouri, A. J. Bidhendi, T. Tani, J. Suzuki, C. Conrad, Y. Chebli, N. Liu, C. Karunakaran, G. Scarcelli, A. Geitmann, *Plant Physiol.* **2019**, *181*, 127; c) K. T. Haas, R. Wightman, E. M. Meyerowitz, A. Peaucelle, *Science* **2020**, *367*, 1003.

[92] A. J. Bidhendi, B. Altartouri, F. P. Gosselin, A. Geitmann, *Cell Rep.* **2019**, *28*, 1237.

[93] J. C. Huss, S. J. Antreich, J. Bachmayr, N. Xiao, M. Eder, J. Konnerth, N. Gierlinger, *Adv. Mater.* **2020**, *32*, 2004519.

[94] W. Zhao, L. Hanson, H.-Y. Lou, M. Akamatsu, P. D. Chowdary, F. Santoro, J. R. Marks, A. Grassart, D. G. Drubin, Y. Cui, *Nat. Nanotechnol.* **2017**, *12*, 750.

[95] R. Mok, J. Dunkel, V. Kantsler, *Phys. Rev. E* **2019**, *99*, 052607.

[96] P. Rougerie, L. Pieuchot, R. S. dos Santos, J. Marteau, M. Bigerelle, P.-F. Chauvy, M. Farina, K. Anselme, *Sci. Rep.* **2020**, *10*, 14784.

[97] S. A. Ruiz, C. S. Chen, *Stem Cells* **2008**, *26*, 2921.

[98] S. Ehrig, B. Schamberger, C. M. Bidan, A. West, C. Jacobi, K. Lam, P. Kollmannsberger, A. Petersen, P. Tomancak, K. Kommareddy, F. D. Fischer, P. Fratzl, J. W. C. Dunlop, *Sci. Adv.* **2019**, *5*, eaav9394.

[99] M. Paris, A. Goetz, I. Hettrich, C. M. Bidan, J. W. C. Dunlop, H. Razi, I. Zizak, D. W. Hutmacher, P. Fratzl, G. N. Duda, W. Wagermaier, A. Cipitria, *Acta Biomater.* **2017**, *60*, 64.

[100] S. W. Cranford, J. de Boer, C. van Blitterswijk, M. J. Buehler, *Adv. Mater.* **2013**, *25*, 802.

[101] Y. Yang, T. Xu, H.-P. Bei, L. Zhang, C.-Y. Tang, M. Zhang, C. Xu, L. Bian, K. W.-K. Yeung, J. Y. H. Fuh, X. Zhao, *Proc. Natl. Acad. Sci. USA* **2022**, *119*, e2206684119.

[102] H. V. Unadkat, M. Hulsman, K. Cornelissen, B. J. Papenburg, R. K. Truckenmüller, A. E. Carpenter, M. Wessling, G. F. Post, M. Uetz, M. J. T. Reinders, D. Stamatialis, C. A. van Blitterswijk, J. de Boer, *Proc. Natl. Acad. Sci. USA* **2011**, *108*, 16565.

[103] a) M. Théry, *J. Cell Sci.* **2010**, *123*, 4201; b) C. D. Bain, G. M. Whitesides, *Angew. Chem.* **1989**, *101*, 522; c) A. Kumar, H. A. Biebuyck, G. M. Whitesides, *Langmuir* **1994**, *10*, 1498.

**ADVANCED
SCIENCE NEWS**

www.advancedsciencenews.com

**ADVANCED
MATERIALS**

www.advmat.de

[104] D. M. Lyra-Leite, A. P. Petersen, N. R. Ariyasinghe, N. Cho, M. L. McCain, *J. Mol. Cell. Cardiol.* **2021**, *150*, 32.

[105] L. Q. Wan, K. Ronaldson, M. Park, G. Taylor, Y. Zhang, J. M. Gimble, G. Vunjak-Novakovic, *Proc. Natl. Acad. Sci. USA* **2011**, *108*, 12295.

[106] S. J. Bryant, J. L. Cuy, K. D. Hauch, B. D. Ratner, *Biomaterials* **2007**, *28*, 2978.

[107] F. Chen, J. Ricken, D. Xu, S. V. Wegner, *Adv. Biosyst.* **2019**, *3*, 1800269.

[108] P. Durand-Smet, T. A. Spelman, E. M. Meyerowitz, H. Jönsson, *Proc. Natl. Acad. Sci. USA* **2020**, *117*, 17399.

[109] V. N. Truskett, M. P. Watts, *Trends Biotechnol.* **2006**, *24*, 312.

[110] a) S. Lee, H. Yang, C. Chen, S. Venkatraman, A. Darsha, S. M. Wu, J. C. Wu, T. Seeger, *J. Visualized Exp.* **2020**, *158*, e60888; b) G. Sahni, J. Yuan, Y.-C. Toh, *J. Visualized Exp.* **2016**, *112*, 54097.

[111] D. J. Guckenberger, T. E. de Groot, A. M. Wan, D. J. Beebe, E. W. Young, *Lab Chip* **2015**, *15*, 2364.

[112] E. Latorre, S. Kale, L. Casares, M. Gómez-González, A. Uroz, L. Valon, R. V. Nair, E. Garreta, N. Montserrat, A. J. N. del Campo, *Nature* **2018**, *563*, 203.

[113] W. Oropallo, L. A. Piegl, *Eng. Comput.* **2016**, *32*, 135.

[114] S. Ravi-Kumar, B. Lies, X. Zhang, H. Lyu, H. Qin, *Polym. Int.* **2019**, *68*, 1391.

[115] G. C. Engelmayr, Jr., M. Cheng, C. J. Bettinger, J. T. Borenstein, R. Langer, L. E. Freed, *Nat. Mater.* **2008**, *7*, 1003.

[116] N. Ahmed, S. Darwish, A. M. Alahmari, *Mater. Manuf. Processes* **2016**, *31*, 1121.

[117] A. Francone, S. Merino, A. Retolaza, J. Ramiro, S. A. Alves, J. V. de Castro, N. M. Neves, A. Arana, J. M. Marimon, C. M. S. Torres, N. Kehagias, *Surf. Interfaces* **2021**, *27*, 101494.

[118] I. Mutreja, T. B. F. Woodfield, S. Sperling, V. Nock, J. J. Evans, M. M. Alkaisi, *Biofabrication* **2015**, *7*, 025002.

[119] H. Elliott, R. S. Fischer, K. A. Myers, R. A. Desai, L. Gao, C. S. Chen, R. S. Adelstein, C. M. Waterman, G. Danuser, *Nat. Cell Biol.* **2015**, *17*, 137.

[120] G. de Vicente, M. C. Lensen, *Eur. Polym. J.* **2016**, *78*, 290.

[121] Z. Li, Y. W. Gong, S. J. Sun, Y. Du, D. Y. Lu, X. F. Liu, M. Long, *Biomaterials* **2013**, *34*, 7616.

[122] S. Yang, K. Khare, P. C. Lin, *Adv. Funct. Mater.* **2010**, *20*, 2550.

[123] C. Tomba, T. Petithory, R. Pedron, A. Airoudj, I. Di Meglio, A. Roux, V. Luchnikov, *Small* **2019**, *15*, 1900162.

[124] C. Tomba, V. Luchnikov, L. Barberi, C. Blanch-Mercader, A. Roux, *Dev. Cell* **2022**, *57*, 1257.

[125] S. L. Arias, J. Devorkin, A. Civantos, J. P. Allain, *Langmuir* **2021**, *37*, 16.

[126] L. Wang, T. J. McCarthy, *Proc. Natl. Acad. Sci. USA* **2015**, *112*, 2664.

[127] J. Nakanishi, Y. Kikuchi, T. Takarada, H. Nakayama, K. Yamaguchi, M. Maeda, *Anal. Chim. Acta* **2006**, *578*, 100.

[128] M. Gabi, A. Larmagnac, P. Schulte, J. Vörös, *Colloids Surf., B* **2010**, *79*, 365.

[129] Y. Kikuchi, J. Nakanishi, T. Shimizu, H. Nakayama, S. Inoue, K. Yamaguchi, H. Iwai, Y. Yoshida, Y. Horiike, T. Takarada, M. Maeda, *Langmuir* **2008**, *24*, 13084.

[130] H. Kamble, M. J. Barton, M. Jun, S. Park, N.-T. Nguyen, *Lab Chip* **2016**, *16*, 3193.

[131] A. S. Gladman, E. A. Matsumoto, R. G. Nuzzo, L. Mahadevan, J. A. Lewis, *Nat. Mater.* **2016**, *15*, 413.

[132] D. G. Tamay, T. Dursun Usal, A. S. Alagoz, D. Yucel, N. Hasirci, V. Hasirci, *Front. Bioeng. Biotechnol.* **2019**, *7*, 164.

[133] a) M. Schaffner, P. A. Rühs, F. Coulter, S. Kilcher, A. R. Studart, *Sci. Adv.* **2017**, *3*, eaao6804; b) S. Balasubramanian, M.-E. Aubin-Tam, A. S. Meyer, *ACS Synth. Biol.* **2019**, *8*, 1564.

[134] H.-Y. Lou, W. Zhao, X. Li, L. Duan, A. Powers, M. Akamatsu, F. Santoro, A. F. McGuire, Y. Cui, D. G. Drubin, *Proc. Natl. Acad. Sci. USA* **2019**, *116*, 23143.

[135] A.-L. Le Roux, X. Quiroga, N. Walani, M. Arroyo, P. Roca-Cusachs, *Philos. Trans. R. Soc., B* **2019**, *374*, 20180221.

[136] C. Luxenburg, R. Zaidel-Bar, *Exp. Cell Res.* **2019**, *378*, 232.

[137] a) A. Ray, O. Lee, Z. Win, R. M. Edwards, P. W. Alford, D.-H. Kim, P. P. Provenzano, *Nat. Commun.* **2017**, *8*, 14923; b) K.-H. Nam, P. Kim, D. K. Wood, S. Kwon, P. P. Provenzano, D.-H. Kim, *Sci. Rep.* **2016**, *6*, 29749; c) G. Ramirez-San Juan, P. Oakes, M. Gardel, *Mol. Biol. Cell* **2017**, *28*, 1043.

[138] M. Werner, N. A. Kurniawan, G. Korus, C. V. C. Bouten, A. Petersen, *J. R. Soc., Interface* **2018**, *15*, 20180162.

[139] N. D. Bade, R. D. Kamien, R. K. Assoian, K. J. Stebe, *Sci. Adv.* **2017**, *3*, e1700150.

[140] J. Y. Park, D. H. Lee, E. J. Lee, S. H. Lee, *Lab Chip* **2009**, *9*, 2043.

[141] M. Werner, S. B. G. Blanquer, S. P. Haimi, G. Korus, J. W. C. Dunlop, G. N. Duda, D. W. Grijpma, A. Petersen, *Adv. Sci.* **2017**, *4*, 1600347.

[142] a) M. Vassaux, L. Pieuchot, K. Anselme, M. Bigerelle, J.-L. Milan, *Biophys. J.* **2019**, *117*, 1136; b) B. Winkler, I. S. Aranson, F. Ziebert, *Commun. Phys.* **2019**, *2*, 82.

[143] E. Sitarska, S. D. Almeida, M. Beckwith, J. Stopp, Y. Schwab, M. Sixt, A. Kreshuk, A. Erzberger, A. Diz-Muñoz, *bioRxiv* **2021**, 2021.03.26.437199.

[144] A. Reversat, F. Gaertner, J. Merrin, J. Stopp, S. Tasciyan, J. Aguilera, I. de Vries, R. Hauschild, M. Hons, M. Piel, A. Callan-Jones, R. Voituriez, M. Sixt, *Nature* **2020**, *582*, 582.

[145] a) A. Lomakin, C. Cattin, D. Cuvelier, Z. Alraies, M. Molina, G. Nader, N. Srivastava, P. Saez, J. Garcia-Arcos, I. Zhitnyak, *Science* **2020**, *370*, eaba2894; b) V. Venturini, F. Pezzano, F. C. Castro, H.-M. Häkkinen, S. Jiménez-Delgado, M. Colomer-Rosell, M. Marro, Q. Tolosa-Ramon, S. Paz-López, M. A. Valverde, *Science* **2020**, *370*, eaba2644.

[146] T. Ostapenko, F. J. Schwarzendahl, T. J. Böddeker, C. T. Kreis, J. Cammann, M. G. Mazza, O. Bäumchen, *Phys. Rev. Lett.* **2018**, *120*, 068002.

[147] O. Sipos, K. Nagy, R. Di Leonardo, P. Galajda, *Phys. Rev. Lett.* **2015**, *114*, 258104.

[148] E. Secchi, A. Vitale, G. L. Miño, V. Kantsler, L. Eberl, R. Rusconi, R. Stocker, *Nat. Commun.* **2020**, *11*, 2851.

[149] B. Szabó, G. J. Szöllösi, B. Gönci, Z. Jurányi, D. Selmeczi, T. Vicsek, *Phys. Rev. E* **2006**, *74*, 061908.

[150] S. Ehrig, J. Ferracci, R. Weinkamer, J. W. C. Dunlop, *Phys. Rev. E* **2017**, *95*, 062609.

[151] S.-Z. Lin, Y. Li, J. Ji, B. Li, X.-Q. Feng, *Soft Matter* **2020**, *16*, 2941.

[152] A. Ravasio, I. Cheddadi, T. Chen, T. Pereira, H. T. Ong, C. Bertocchi, A. Brugues, A. Jacinto, A. J. Kabla, Y. Toyama, X. Trepat, N. Gov, L. Neves de Almeida, B. Ladoux, *Nat. Commun.* **2015**, *6*, 7683.

[153] C. M. Nelson, R. P. Jean, J. L. Tan, W. F. Liu, N. J. Sniadecki, A. A. Spector, C. S. Chen, *Proc. Natl. Acad. Sci. USA* **2005**, *102*, 11594.

[154] T. Chen, A. Callan-Jones, E. Fedorov, A. Ravasio, A. Brugués, H. T. Ong, Y. Toyama, B. C. Low, X. Trepat, T. Shemesh, R. Voituriez, B. Ladoux, *Nat. Phys.* **2019**, *15*, 393.

[155] L. Juignet, B. Charbonnier, V. Dumas, W. Bouleftour, M. Thomas, C. Laurent, L. Vico, N. Douard, D. Marchat, L. Malaval, *Acta Biomater.* **2017**, *53*, 536.

[156] C. M. Nelson, *Biochim. Biophys. Acta* **2009**, *1793*, 903.

[157] S. Callens, D. Fan, I. van Hengel, M. Minneboo, L. Fratila-Apachitei, A. Zadpoor, *bioRxiv* **2020**.

[158] T. Yamashita, P. Kollmannsberger, K. Mawatari, T. Kitamori, V. Vogel, *Acta Biomater.* **2016**, *45*, 85.

[159] W. Xi, S. Sonam, T. Beng Saw, B. Ladoux, C. Teck Lim, *Nat. Commun.* **2017**, *8*, 1517.

[160] H. G. Yevick, G. Duclos, I. Bonnet, P. Silberzan, *Proc. Natl. Acad. Sci. USA* **2015**, *112*, 5944.

[161] M. B. Mazalan, M. A. B. Ramlan, J. H. Shin, T. Ohashi, *Micromachines* **2020**, *11*, 659.

[162] F. A. Maechler, C. Allier, A. Roux, C. Tomba, *J. Cell Sci.* **2019**, *132*, jcs222372.

[163] S. M. Yu, J. M. Oh, J. Lee, W. Lee-Kwon, W. Jung, F. Amblard, S. Granick, Y. K. Cho, *Acta Biomater.* **2018**, *77*, 311.

[164] M. Cetera, G. R. Ramirez-San Juan, P. W. Oakes, L. Lewellyn, M. J. Fairchild, G. Tanentzapf, M. L. Gardel, S. Horne-Badovinac, *Nat. Commun.* **2014**, *5*, 5511.

[165] A. Glentis, C. Blanch-Mercader, L. Balasubramaniam, T. B. Saw, J. d'Alessandro, S. Janel, A. Douanier, B. Delaval, F. Lafont, C. T. Lim, D. Delacour, J. Prost, W. Xi, B. Ladoux, *Sci. Adv.* **2022**, *8*, eabn5406.

[166] W. Tang, A. Das, A. F. Pegoraro, Y. L. Han, J. Huang, D. A. Roberts, H. Yang, J. J. Fredberg, D. N. Kotton, D. Bi, M. Guo, *Nat. Phys.* **2022**, *18*, 1371.

[167] D. Stopak, A. K. Harris, *Dev. Biol.* **1982**, *90*, 383.

[168] a) M. Rumpler, A. Woesz, J. W. Dunlop, J. T. van Dongen, P. Fratzl, *J. R. Soc., Interface* **2008**, *5*, 1173; b) C. M. Bidan, K. P. Kommareddy, M. Rumpler, P. Kollmannsberger, Y. J. M. Brechet, P. Fratzl, J. W. C. Dunlop, *PLoS One* **2012**, *7*, e36336.

[169] a) J. Knychala, N. Bouropoulos, C. J. Catt, O. L. Katsamenis, C. P. Please, B. G. Sengers, *Ann. Biomed. Eng.* **2013**, *41*, 917; b) P. Joly, G. N. Duda, M. Schone, P. B. Welzel, U. Freudenberg, C. Werner, A. Petersen, *PLoS One* **2013**, *8*, e73545.

[170] C. M. Bidan, K. P. Kommareddy, M. Rumpler, P. Kollmannsberger, P. Fratzl, J. W. C. Dunlop, *Adv. Healthcare Mater.* **2013**, *2*, 186.

[171] C. M. Bidan, P. Kollmannsberger, V. Gering, S. Ehrig, P. Joly, A. Petersen, V. Vogel, P. Fratzl, J. W. Dunlop, *J. R. Soc., Interface* **2016**, *13*, 20160136.

[172] A. A. Zadpoor, *Biomater. Sci.* **2015**, *3*, 231.

[173] I. Papantoniou, Y. Guyot, M. Sonnaert, G. Kerckhofs, F. P. Luyten, L. Geris, J. Schrooten, *Biotechnol. Bioeng.* **2014**, *111*, 2560.

[174] Y. Guyot, I. Papantoniou, F. P. Luyten, L. Geris, *Biomech. Model. Mechanobiol.* **2016**, *15*, 169.

[175] a) J. R. Vetsch, R. Müller, S. Hofmann, *J. R. Soc., Interface* **2016**, *13*, 20160425; b) M. Rubert, J. R. Vetsch, I. Lehtoviita, M. Sommer, F. Zhao, A. R. Studart, R. Müller, S. Hofmann, *Tissue Eng. Part A* **2021**, *27*, 1192.

[176] A. Berner, M. A. Woodruff, C. X. F. Lam, M. T. Arafat, S. Saifzadeh, R. Steck, J. Ren, M. Nerlich, A. K. Ekaputra, I. Gibson, D. W. Hutmacher, *Int. J. Oral Surg.* **2014**, *43*, 506.

[177] M. Hallman, J. A. Driscoll, R. Lubbe, S. Jeong, K. Chang, M. Haleem, A. Jakus, R. Pahapill, C. Yun, R. Shah, *Tissue Eng. Part A* **2021**, *27*, 26.

[178] a) A. P. G. Castro, J. Santos, T. Pires, P. R. Fernandes, *Macromol. Mater. Eng.* **2020**, *305*, 2000487; b) C. Perier-Metz, G. N. Duda, S. Checa, *Front. Bioeng. Biotechnol.* **2020**, *8*, 585799.

[179] D. Van hede, B. Liang, S. Anania, M. Barzegari, B. Verlée, G. Nolens, J. Pirson, L. Geris, F. Lambert, *Adv. Funct. Mater.* **2022**, *32*, 2105002.

[180] P. Kollmannsberger, C. Bidan, J. Dunlop, P. Fratzl, *Soft Matter* **2011**, *7*, 9549.

[181] a) Y. Guyot, F. P. Luyten, J. Schrooten, I. Papantoniou, L. Geris, *Biotechnol. Bioeng.* **2015**, *112*, 2591; b) P. F. Egan, K. A. Shea, S. J. Ferguson, *Biomech. Model. Mechanobiol.* **2018**, *17*, 1481.

[182] P. R. Buenzli, M. Lanaro, C. S. Wong, M. P. McLaughlin, M. C. Allenby, M. A. Woodruff, M. J. Simpson, *Acta Biomater.* **2020**, *114*, 285.

[183] C. Pérez-González, G. Ceada, M. Matejčić, X. Trepat, *Curr. Opin. Genet. Dev.* **2022**, *72*, 82.

[184] A. Dekanty, M. Milán, *EMBO Rep.* **2011**, *12*, 1003.

[185] S. Sick, S. Reinker, J. Timmer, T. Schlake, *Science* **2006**, *314*, 1447.

[186] T.-X. Jiang, H.-S. Jung, R. B. Widelitz, C.-M. Chuong, *Development* **1999**, *126*, 4997.

[187] C. Chang, P. Wu, R. E. Baker, P. K. Maini, L. Alibardi, C.-M. Chuong, *Int. J. Dev. Biol.* **2009**, *53*, 813.

[188] A. M. Turing, *Philos. Trans. R. Soc. London, Ser. B* **1952**, *237*, 37.

[189] K. S. Stapornwongkul, J.-P. Vincent, *Nat. Rev. Genet.* **2021**, *22*, 393.

[190] A. Mietke, F. Jülicher, I. F. Sbalzarini, *Proc. Natl. Acad. Sci. USA* **2019**, *116*, 29.

[191] R. R. Molina, S. Liese, A. Carlson, *Biophys. J.* **2021**, *120*, 424.

[192] I. Heemskerk, *Dev. Biol.* **2020**, *460*, 86.

[193] M. C. Milinkovitch, L. Manukyan, A. Debry, N. Di-Poï, S. Martin, D. Singh, D. Lambert, M. Zwicker, *Science* **2013**, *339*, 78.

[194] L. Hubatsch, N. W. Goehring, *Curr. Top. Dev. Biol.* **2020**, *137*, 247.

[195] E. Hannezo, B. Dong, P. Recho, J.-F. Joanny, S. Hayashi, *Proc. Natl. Acad. Sci. U. S. A.* **2015**, *112*, 8620.

[196] N. Barker, J. H. van Es, J. Kuipers, P. Kujala, M. van den Born, M. Cozijnsen, A. Haegebarth, J. Korving, H. Begthel, P. J. Peters, H. Clevers, *Nature* **2007**, *449*, 1003.

[197] A. E. Shyer, T. R. Huycke, C. Lee, L. Mahadevan, C. J. Tabin, *Cell* **2015**, *161*, 569.

[198] K. D. Sumigray, M. Terwilliger, T. Lechler, *Dev. Cell* **2018**, *45*, 183.

[199] Q. Yang, S.-L. Xue, C. J. Chan, M. Rempfler, D. Vischi, F. Maurer-Gutierrez, T. Hiiragi, E. Hannezo, P. Liberali, *Nat. Cell Biol.* **2021**, *23*, 733.

[200] a) W. Xi, J. Saleh, A. Yamada, C. Tomba, B. Mercier, S. Janel, T. Dang, M. Soleilhac, A. Djemat, H. Wu, B. Romagnolo, F. Lafont, R.-M. Mège, Y. Chen, D. Delacour, *Biomaterials* **2022**, *282*, 121380; b) N. Gjorevski, M. Nikolaev, T. E. Brown, O. Mitrofanova, N. Brandenberg, F. W. DelRio, F. M. Yavitt, P. Liberali, K. S. Anseth, M. P. Lutolf, *Science* **2022**, *375*, eaaw9021.

[201] C. A. Thorne, I. W. Chen, L. E. Sanman, M. H. Cobb, L. F. Wu, S. J. Altschuler, *Dev. Cell* **2018**, *44*, 624.

[202] L. M. C. Janssen, A. Kaiser, H. Löwen, *Sci. Rep.* **2017**, *7*, 5667.

[203] S. Shankar, M. J. Bowick, M. C. Marchetti, *Phys. Rev. X* **2017**, *7*, 031039.

[204] a) F. C. Keber, E. Loiseau, T. Sanchez, S. J. DeCamp, L. Giomi, M. J. Bowick, M. C. Marchetti, Z. Dogic, A. R. Bausch, *Science* **2014**, *345*, 1135; b) J. A. Santiago, *Phys. Rev. E* **2018**, *97*, 052706; c) Z. You, D. J. G. Pearce, A. Sengupta, L. Giomi, *Phys. Rev. Lett.* **2019**, *123*, 178001; d) J. Dhar, A. L. P. Thai, A. Ghoshal, L. Giomi, A. Sengupta, *Nat. Phys.* **2022**, *18*, 945.

[205] Q. Zhang, J. Li, J. Nijjer, H. Lu, M. Kothari, R. Alert, T. Cohen, J. Yan, *Proc. Natl. Acad. Sci. USA* **2021**, *118*, e2107107118.